Cell Reports
Medicine

Article

Modulation of TCR stimulation and pifithrin-α improves the genomic safety profile of CRISPR-engineered human T cells

Graphical abstract

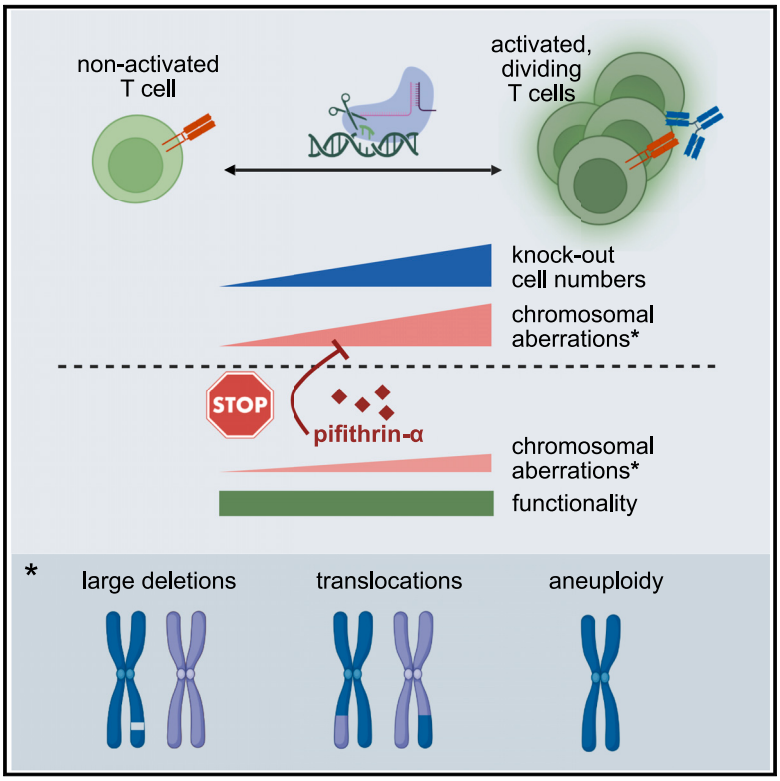

Highlights

- Stronger T cell activation results in larger deletions during CRISPR editing
- Addition of pifithrin-α reduces large deletions, translocations, and aneuploidy
- Pifithrin-α acts in a p53-independent manner and maintains T cell functionality
- Improved safety of T cell products by pifithrin-α and control of TCR stimulation

Authors

Laurenz T. Ursch, Jule S. Müschen, Julia Ritter, ..., Dirk H. Busch, Toni Cathomen, Kathrin Schumann

Correspondence

kathrin.schumann@tum.de

In brief

Ursch et al. describe TCR activation and cell proliferation as cell-intrinsic driving forces for chromosomal aberrations in CRISPR-edited human T cells. Modulation of TCR stimulation and the addition of the small-molecule pifithrin-α improve the genomic safety profile of CRISPR-engineered human T cells.

Ursch et al., 2024, Cell Reports Medicine *5*, 101846
December 17, 2024
https://doi.org/10.1016/j.xcrm.2024.101846

CellPress

Cell Reports Medicine

CellPress
OPEN ACCESS

Article

Modulation of TCR stimulation and pifithrin-α improves the genomic safety profile of CRISPR-engineered human T cells

Laurenz T. Ursch,[1,12] Jule S. Müschen,[1,12] Julia Ritter,[1] Julia Klermund,[2,3] Bettina E. Bernard,[1] Saskia Kolb,[1] Linda Warmuth,[1] Geoffroy Andrieux,[4,5] Gregor Miller,[6] Marina Jiménez-Muñoz,[6] Fabian J. Theis,[7,8] Melanie Boerries,[4,5,9] Dirk H. Busch,[1,10] Toni Cathomen,[2,3,5] and Kathrin Schumann[1,11,13,*]

[1]Technical University of Munich (TUM), School of Medicine and Health, Department of Preclinical Medicine, Institute for Medical Microbiology, Immunology and Hygiene, 81675 Munich, Germany
[2]Institute for Transfusion Medicine and Gene Therapy, Medical Center – University of Freiburg, 79106 Freiburg, Germany
[3]Center for Chronic Immunodeficiency (CCI), Medical Center – University of Freiburg, 79106 Freiburg, Germany
[4]Institute of Medical Bioinformatics and Systems Medicine, Medical Center – University of Freiburg, Freiburg, Germany
[5]Faculty of Medicine, University of Freiburg, 79106 Freiburg, Germany
[6]Core Facility Statistical Consulting, Helmholtz Zentrum München, 85764 Neuherberg, Germany
[7]Institute of Computational Biology, Helmholtz Zentrum München, 85764 Neuherberg, Germany
[8]School of Computing, Information and Technology, Technical University of Munich, 85748 Garching, Germany
[9]German Cancer Consortium (DKTK), Partner site Freiburg, a partnership between DKFZ and Medical Center - University of Freiburg, 79106 Freiburg, Germany
[10]German Center for Infection Research, Deutsches Zentrum für Infektionsforschung (DZIF), Partner Site Munich, 81675 Munich, Germany
[11]TUM, Institute for Advanced Study, 85748 Garching, Germany
[12]These authors contributed equally
[13]Lead contact
*Correspondence: kathrin.schumann@tum.de
https://doi.org/10.1016/j.xcrm.2024.101846

SUMMARY

CRISPR-engineered chimeric antigen receptor (CAR) T cells are at the forefront of novel cancer treatments. However, several reports describe the occurrence of CRISPR-induced chromosomal aberrations. So far, measures to increase the genomic safety of T cell products focused mainly on the components of the CRISPR-Cas9 system and less on T cell-intrinsic features, such as their massive expansion after T cell receptor (TCR) stimulation. Here, we describe driving forces of indel formation in primary human T cells. Increased T cell activation and proliferation speed correlate with larger deletions. Editing of non-activated T cells reduces the risk of large deletions with the downside of reduced knockout efficiencies. Alternatively, the addition of the small-molecule pifithrin-α limits large deletions, chromosomal translocations, and aneuploidy in a p53-independent manner while maintaining the functionality of CRISPR-engineered T cells, including CAR T cells. Controlling T cell activation and pifithrin-α treatment are easily implementable strategies to improve the genomic integrity of CRISPR-engineered T cells.

INTRODUCTION

CRISPR-Cas9 editing of primary human T cells opened new avenues for engineered adoptive T cell therapies tackling cancer or HIV infection.[1–4] T cells can now be equipped with high-affinity chimeric antigen receptors (CARs) or T cell receptors (TCRs) using CRISPR-Cas9-mediated knockins (KIs) without the need for viral transduction.[1,2] Besides that, CRISPR-Cas9 knockouts (KOs) of co-inhibitory receptors can boost T cell effector functions and increase the efficiency of adoptive T cell therapies.[1,5,6] In 2020, June and colleagues published the first clinical CRISPR-Cas9 trial in humans, infusing TCRα TCRβ PD-1 triple KO CAR T cells into patients with refractory cancer. Although the trial was a success, up to 4% of these KO T cells carried chromosomal translocations or truncations.[1] In an independent clinical trial, Foy et al. used CRISPR-Cas9 engineering to ablate both TCR chains while simultaneously introducing a neoantigen TCR into the *TRAC* locus. Also, in this trial, chromosomal translocations were detectable in the final T cell products.[2] Further studies described the occurrence of large deletions spanning from 50 bp up to several kb or even aneuploidy in diverse cell types after CRISPR-Cas9 editing including T cells.[7–11] T cells with such chromosomal abnormalities can withstand *ex vivo* expansion protocols and are, therefore, an ongoing concern for CRISPR-Cas9-engineered T cell products in the clinic.[1,10]

Different approaches have been developed to reduce the risks of large deletions such as algorithms predicting the indel pattern

Please cite this article in press as: Ursch et al., Modulation of TCR stimulation and pifithrin-α improves the genomic safety profile of CRISPR-engineered human T cells, Cell Reports Medicine (2024), https://doi.org/10.1016/j.xcrm.2024.101846

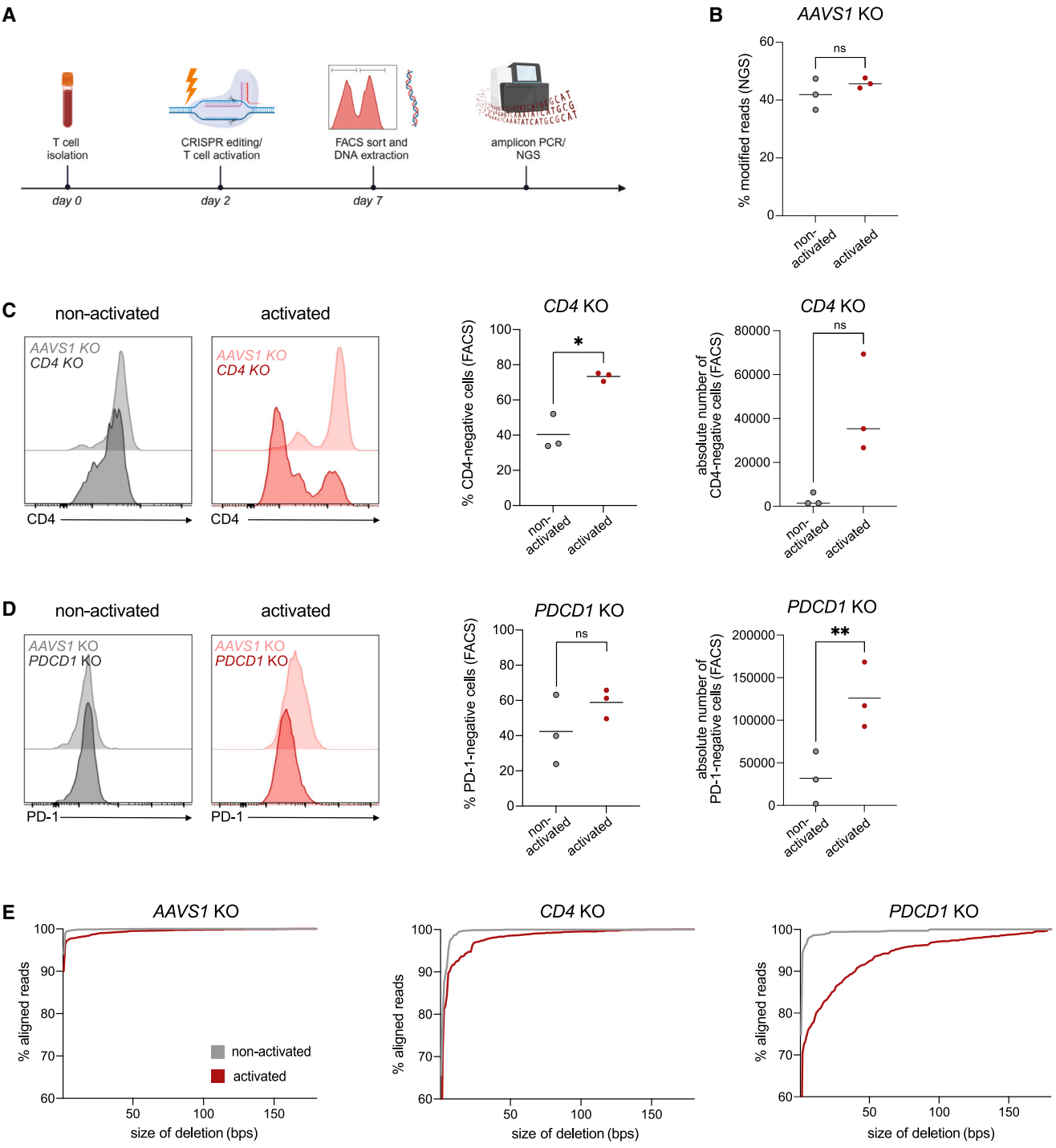

Figure 1. CRISPR-Cas9-induced deletion patterns in non-activated and activated human CD4 T cells

(A) Schematic workflow of CRISPR-Cas9 editing experiments.

(B) Percentage of indel formation at the *AAVS1* gene locus determined by amplicon NGS sequencing. *n*(*AAVS1*) = 3, biological replicates.

(C) Characterization of *CD4* KO T cells. Left: representative flow cytometry plots of CD4 protein expression in *AAVS1* KO control and *CD4* KO T cells without (gray) or with TCR stimulation (red) after CRISPR-Cas9 editing. Right: quantification of CD4 expression and absolute numbers of CD4-negative cells in non-activated and activated CD4 T cells by flow cytometry analysis. *n*(*CD4*) = 3, biological replicates.

(legend continued on next page)

Please cite this article in press as: Ursch et al., Modulation of TCR stimulation and pifithrin-α improves the genomic safety profile of CRISPR-engineered human T cells, Cell Reports Medicine (2024), https://doi.org/10.1016/j.xcrm.2024.101846

at target sites or base and prime editing, which only introduce DNA single-strand cuts.[12–16] However, successful T cell engineering is not always achievable with these alternatives due to reduced KO rates or limitations in KI sizes. Importantly, large KIs for the introduction of CARs or TCRs into the intrinsic *TRAC* locus of human T cells are strictly dependent on Cas9-induced DNA double-strand breaks (DSBs).[17] Inhibition of the non-homologous end joining pathway (NHEJ) or addition of DNA templates can limit the risk of large deletions by engaging the homology-directed DNA repair pathway (HDR).[18–20] But enabling HDR cannot abolish this risk completely.[18,19] To develop safer, alternative CRISPR engineering strategies for human T cells, we need a better understanding of their cell-intrinsic driving forces that shape indel patterns. In general, non-proliferative T cells are more prone to undergo apoptosis after DNA damage, for example, induced by radiation because of inactive DNA repair pathways, whereas T cells undergoing fast cell divisions have a higher risk of accumulating DNA damage.[21,22] A potential link between DNA damage and T cell proliferation is the tumor suppressor p53. Upon Cas9-induced DNA damage, p53 is activated resulting in cell-cycle arrest and activation of DNA repair.[23,24] Interestingly, TCR stimulation results in reduced p53 protein levels.[25] Interfering with p53 function could thereby potentially boost deletion sizes in human T cells.

Here, we systematically analyzed the influence of TCR stimulation and T cell proliferation on the CRISPR-Cas9 editing outcome. Our findings show that TCR stimulation and high cell proliferation speed result in high KO rates with the downside of larger deletions. Gene ablation in non-activated T cells is less efficient, but the induced insertions and deletions (indels) are smaller at the target sites. Alternatively, large deletions, chromosomal rearrangements, and copy-number variations can be reduced by the addition of the small-molecule cyclic pifithrin-α (PFT-α). Importantly, PFT-α conserved key features of CRISPR-engineered T cells such as cytokine secretion, the composition of T cell subsets, and tumor cell killing *in vitro* and *in vivo*. Controlling T cell activation and the addition of PFT-α are easily accessible strategies to improve the genomic safety profile of CRISPR-Cas9-engineered human T cells.

RESULTS

T cell activation determines CRISPR-Cas9 editing outcomes

Most CRISPR-Cas9 editing protocols targeting human T cells put an emphasis on the optimization of T cell survival, maximum expansion after editing, and KO efficiency. A crucial determinant for the success of these protocols is the timing and strength of the TCR stimulation.[7,17,26] We asked if T cell stimulation affects not only the editing efficiency but also potentially indel patterns. Therefore, we compared the editing outcome in non-activated and activated human CD4 T cells by targeting the safe-harbor locus *AAVS1*, the constitutively expressed surface receptor CD4, and the activation-dependent co-inhibitory receptor PD-1 (corresponding gene: *PDCD1*) with Cas9 ribonucleoproteins (Cas9 RNPs), a method that has already been implemented into clinical protocols.[1,2]

T cells were isolated out of the blood of healthy donors and split after Cas9 RNP nucleofection into two conditions: non-activated or stimulated with anti-CD3/CD28-coated beads. After 4 days, the CD4 and PD-1 protein levels were determined by flow cytometry (gating strategy: Figures S1B and S1C). *AAVS1* KO efficiency was analyzed on the DNA level by amplicon PCR followed by next-generation sequencing (NGS) (Figure 1A, flow sorting strategy for live $CD4^+$ *AAVS1* KO T cells: Figure S1A). We observed reduced percentages of KO cells in non-activated T cells compared to their activated counterparts at the *CD4* locus and tendencies toward reduced indel formation at the other two gene loci (Figures 1B–1D). Differences in PD-1-negative cell numbers determined by flow cytometry between activated and non-activated T cells were less pronounced compared to *CD4*-targeting conditions, because of a relatively high proportion of PD-1-negative T cells in the unstimulated conditions (Figures 1C and 1D). We quantified the absolute number of KO cells in the *CD4* and *PDCD1*-targeting conditions. More efficient gene ablation and cell expansion upon TCR stimulation resulted in higher absolute numbers of KO cells in the activated T cell conditions (Figures 1C and 1D).

Next, we tested if the activation status of the T cells also affected the indel patterns at the target sites. Therefore, the respective KO cells were flow sorted, and DNA was isolated and analyzed by amplicon PCR followed by NGS (flow cytometry sorting strategies for individual KO T cells: Figure S1). This experimental setup allows the detection of up to 180 bp indels. Non-activated T cells had significantly smaller deletions compared to their activated counterparts in all three tested loci. In case of *AAVS1* KOs, no sort enrichment was possible and therefore the overall detected KO efficiencies were lower (Figure 1E). Differences in deletion sizes were more prominent in the activation-dependent gene locus *PDCD1* compared to the constitutively expressed *CD4* locus or in the safe-harbor locus *AAVS1* (Figure 1E, statistics: Table S2). In activated *PDCD1*-targeted T cells, 7.4% of all reads carried deletions larger than 50 bp, compared to 1.4% and 0.5% in the *CD4* and the *AAVS1* loci, respectively (Table S2). We observed similar tendencies for insertions at the *PDCD1* gene locus, but due to the overall very low insertion rates, these effects were less pronounced (Figures S1E–S1G; Table S2). Therefore, we focused our analysis on deletions. Overall, the T cell activation status strongly influences the deletion pattern and TCR stimulation increases the risk of large deletions.

(D) Flow cytometry analysis of *PDCD1* KO T cells. Left: representative flow cytometry plots for PD-1 expression levels in *PDCD1* KO and *AAVS1* KO CD4 T cells (gray: non-activated T cells, red: activated T cells). Right: quantification of PD-1 expression levels and absolute cell numbers for PD-1-negative cells. $n(PDCD1) = 3$, biological replicates.

(B–D) The respective means are indicated. Paired t test, ns: not significant, $^*p < 0.05$, $^{**}p < 0.01$.

(E) Deletion sizes in CRISPR-Cas9-edited T cells at the *AAVS1*, *CD4*, or *PDCD1* target loci in non-activated or activated T cells of the same donors (gray: non-activated; red: activated). Deletion patterns were analyzed by amplicon NGS sequencing. $n(AAVS1, CD4, PDCD1) = 3$, biological replicates.

Please cite this article in press as: Ursch et al., Modulation of TCR stimulation and pifithrin-α improves the genomic safety profile of CRISPR-engineered human T cells, Cell Reports Medicine (2024), https://doi.org/10.1016/j.xcrm.2024.101846

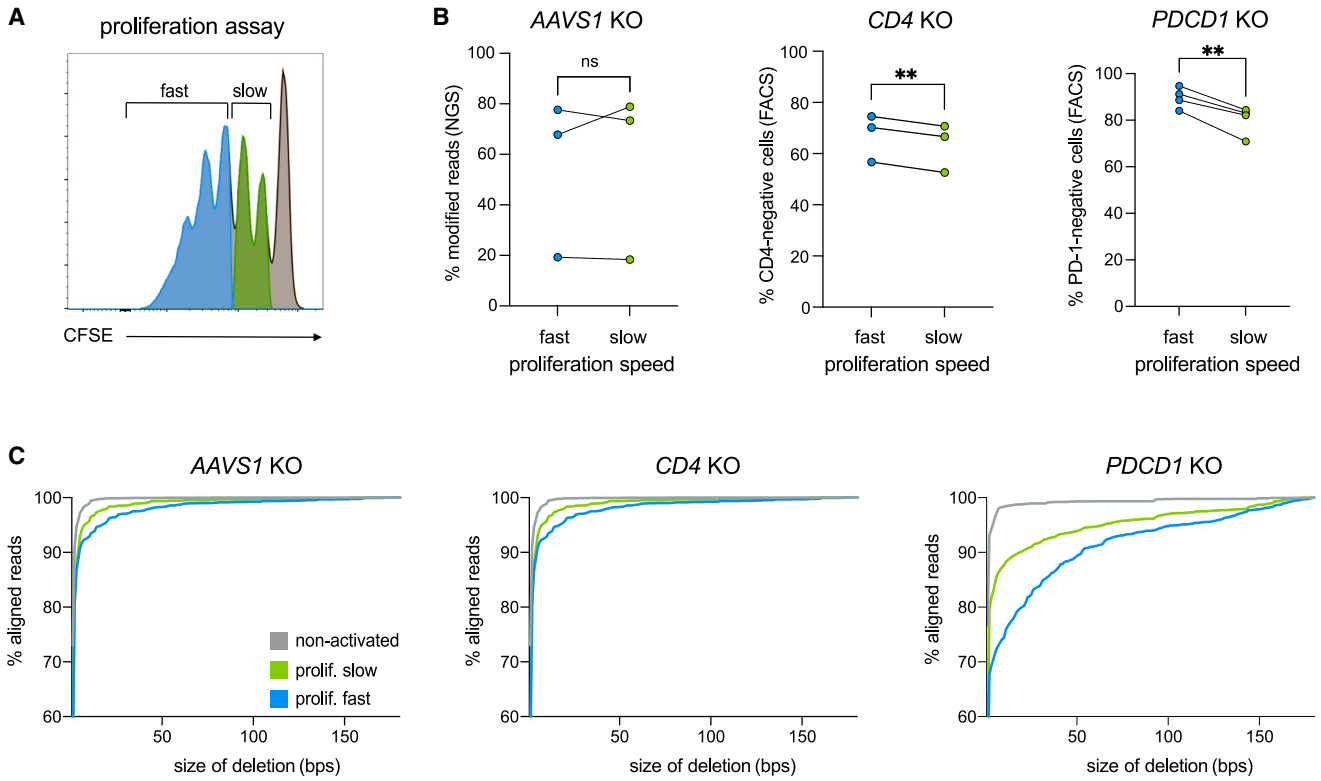

Figure 2. Deletion sizes in CRISPR-Cas9-edited T cells correlate with cell proliferation speed

(A) Representative example of flow cytometry gating strategy for the characterization and isolation of fast (blue) and slowly (green) proliferating CD4 T cells based on CFSE dilution pattern. Non-dividing cells were excluded from the analysis (gray peak on the right).

(B) *AAVS1* indel frequencies (NGS) and CD4 (flow cytometry) and PD-1 KO (flow cytometry) efficiencies in slowly and fast-dividing CD4 T cells based on CFSE dilution pattern. Paired t test, ns: not significant, $^{**}p < 0.01$.

(C) Quantification of deletion sizes dependent on the T cell proliferation speed based on amplicon NGS data.

(B and C) $n(AAVS1) = 3$, $n(CD4) = 3$, $n(PDCD1) = 4$, biological replicates.

High T cell proliferation speed correlates with larger deletion sizes

Upon activation, T cells undergo massive cell proliferation and are more prone to accumulate DNA damage during this expansion phase.[22] Thus, we hypothesize that highly proliferating T cells carry an increased risk of acquiring large deletions during CRISPR-Cas9 editing. To test this hypothesis, CD4 T cells were labeled with the cell proliferation dye CFSE, nucleofected with Cas9 RNPs, activated, and sorted by flow cytometry based on KO phenotype (for CD4 and PD-1) and CFSE dilution pattern 4 days later (Figure 2A; gating strategy: Figures S1A–S1C). Again, fast-proliferating cells, which underwent more cell divisions in a given time, and slowly dividing cells were compared to non-activated cells. The CD4 and PD-1 KO rates determined based on flow cytometry were higher in fast-dividing cells compared to slowly dividing cells. *AAVS1* KO cells, which cannot be sort enriched for KO phenotype, did not show clear differences in KO efficiencies based on cell proliferation (Figure 2B). NGS analyses demonstrated a strong correlation between deletion sizes and cell proliferation speed. Fast-dividing cells accumulated larger deletions, whereas in cells with slower cell cycle speeds, the deletion pattern was more constrained. These effects were conserved in all three target loci (Figure 2C; Table S2). We observed again the strongest effects in cells in which the activation-dependent marker PD-1 was targeted. Here, the deletion sizes varied more and resulted in 10.4% NGS reads with a deletion size larger than 50 bp in fast-dividing cells compared to 6% in slowly dividing cells and 0.7% in non-activated *PDCD1* KO cells (Figure 2C; Table S2). Together, the induction of T cell activation and proliferation results in the generation of higher KO rates with the trade-off of less homogenous, larger deletion sizes.

Chemical p53 inhibition during CRISPR-Cas9 editing of human T cells

Upon DSBs, the transcription factor p53 is activated and in turn triggers DNA repair, cell-cycle arrest, and—depending on the degree of DNA damage—apoptosis.[27] Based on these known functions of p53 also in the context of CRISPR editing, we hypothesized that transient inhibition of p53 during DNA repair of CRISPR-Cas9-induced DSBs will result in higher KO efficiencies and larger deletions.[28]

We independently tested two p53 inhibitors, cyclic-PFT-α and pifithrin-μ (PFT-μ). PFT-α has been described as a reversible inhibitor of p53-mediated apoptosis and p53-dependent gene transcription, whereas PFT-μ specifically blocks p53 interaction

Please cite this article in press as: Ursch et al., Modulation of TCR stimulation and pifithrin-α improves the genomic safety profile of CRISPR-engineered human T cells, Cell Reports Medicine (2024), https://doi.org/10.1016/j.xcrm.2024.101846

CellPress
OPEN ACCESS

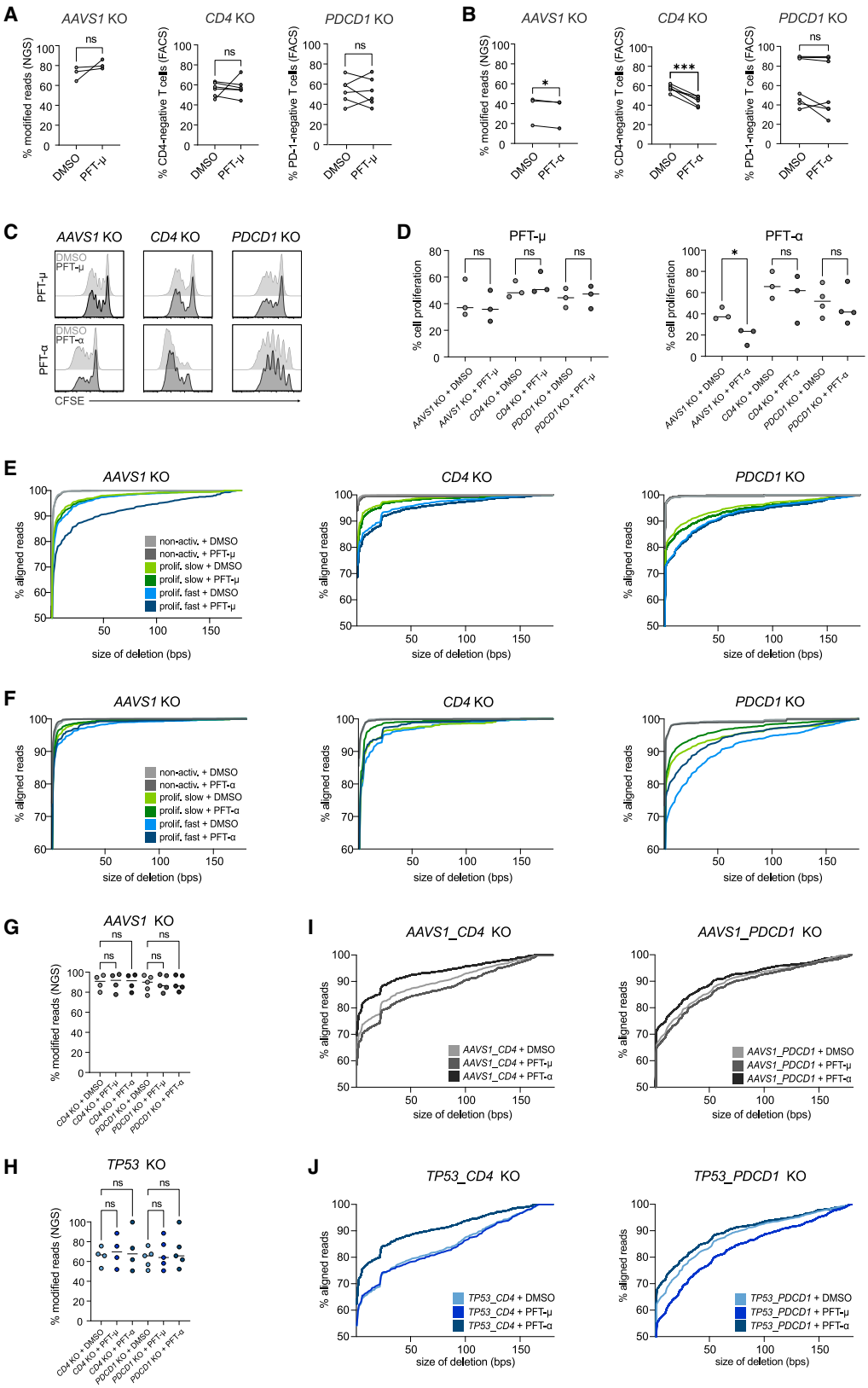

(legend on next page)

Please cite this article in press as: Ursch et al., Modulation of TCR stimulation and pifithrin-α improves the genomic safety profile of CRISPR-engineered human T cells, Cell Reports Medicine (2024), https://doi.org/10.1016/j.xcrm.2024.101846

with the proapoptotic proteins Bcl-xL and Bcl-2 and the translocation of p53 to mitochondria.[29–33] We again targeted *AAVS1*, *CD4*, and *PDCD1* in non-activated and activated T cells, sorted into slowly and fast-dividing cells. With PFT-μ, we did not observe changes in KO frequencies in activated T cells for the targeted gene loci (Figure 3A). The targeting of *AAVS1* and *CD4* in the presence of PFT-α, however, impaired gene KO efficacy, whereas PD-1 KO levels were not affected (Figure 3B). Next, we assessed the impact of p53 inhibitors on cell division rates after TCR stimulation. Adding PFT-μ did not impair T cell proliferation, whereas PFT-α slightly reduced cell division speed in *AAVS1*-edited T cells (Figures 3C and 3D). To test the impact of p53 inhibition on deletion formation, we performed amplicon NGS sequencing. In activated T cells treated with PFT-μ and sorted into slowly and fast-dividing cells, we observed slightly larger deletion sizes in proliferating T cells, with the strongest effect in fast proliferating *AAVS1*-targeted cells (Figure 3E; Table S2). These results align with known functions of p53 in DNA damage repair.[27] However, we observed the opposite effect, a reduction in deletion sizes, in PFT-α-treated activated cells. This effect was consistent in all three genetic loci in slowly as well as in fast-dividing T cells but most pronounced in the *PDCD1*-targeting conditions (Figure 3F; Table S2).

PFT-α and PFT-μ are both widely marketed as p53 inhibitors, but some reports question the specificity of PFT-α. Several alternative PFT-α targets have been proposed, including the aryl hydrocarbon receptor, caspase-3, and cyclin D1.[29–32,34–36] To test if PFT-μ and PFT-α are *bona fide* p53 inhibitors, we challenged the two inhibitors in p53 KO human T cells. We first targeted either *AAVS1* as a negative control or p53 (gene *TP53*) using Cas9 RNPs and rested the T cells for 7 days before performing a second CRISPR KO. For the second KO, we ablated either CD4 or PD-1 while treating the cells with DMSO, PFT-μ, or PFT-α. The KO efficiencies at the *AAVS1* and *TP53* loci were unaffected by the second KO and inhibitor treatment (Figures 3G and 3H). In *TP53* KO conditions, deletions sizes were increased, supporting our initial assumption that loss of p53 results in impaired DNA repair and larger deletions. For example, 20.81% of *TP53_CD4* KO cells carried deletions larger than 50 bp, whereas in *AAVS1_CD4* KO cells, 50 bp deletions only occurred in 12.84% of the cells (Table S2). *AAVS1_CD4* and *AAVS1_PDCD1* KO cells challenged with the two inhibitors recapitulated largely previous observations: treatment with PFT-μ increased deletion sizes. However, PFT-α had the opposite effect. The addition of PFT-α reduced the deletion sizes in both loci tested independent of prior *AAVS1* or *TP53* editing (Figures 3I and 3J; Table S2). These results indicate p53-independent targets of PFT-α in our experimental setup, as this inhibitor can counteract the functional downstream effects of p53 KO. By applying PFT-μ and PFT-α, the deletion size can be shifted to either larger or to smaller, more homogenous deletions.

Subset composition and cytokine profile of PFT-α-treated T cells

To potentially apply PFT-α in clinical T cell engineering protocols, the cellular functionality of the cells after inhibitor treatments must be ensured. We, therefore, determined the potential influences of PFT-α on the expansion capacities, cytokine profile, and the T cell subset composition during extended cell cultivation of up to 9 days. We ablated the constitutively and stably expressed HIV co-receptor CXCR4 as a therapy-relevant target in CD4 T cells (Figure S2A).[4] PFT-α reduced deletion sizes at the *CXCR4* locus while maintaining KO efficiency, absolute KO cell numbers, and cell proliferation (Figures S2B–S2F; Table S2). Different phenotypic parameters of PFT-α-treated *CXCR4* KO cells were compared to cells nucleofected with either non-targeting (NT) or *AAVS1* Cas9 RNPs (gating strategy for *AAVS1* and *CXCR4* KO T cells: Figures S1A and S1D). NT controls were included to assess the actual impact of DSBs in combination with PFT-α on T cell features. *AAVS1* KO T cells served as a control to distinguish potential *CXCR4* gene locus-specific from general KO effects. The T cell subset composition of naive T cells (TN), effector memory T cells (TEM), central memory T cells (TCM), and effector memory CD45RA+ T cells (TEMRA) assessed by CCR7/CD45RA staining was not affected by the inhibitor or the respective nucleofection conditions (TN: CCR7+ CD45RA+, TEM: CCR7− CD45RA−, TCM: CCR7+ CD45RA−, and TEMRA: CCR7− CD45RA+; Figure S2G). IFNγ, IL-2, and TNF-α cytokine levels were unaltered in all tested conditions (Figure S2H).

Figure 3. Deletion sizes after CRISPR-Cas9 editing in the presence of PFT-μ or PFT-α

(A) NGS analysis of *AAVS1* indel frequencies and flow cytometry analysis of CD4 and PD-1 KO efficiencies in activated CD4 T cells treated with DMSO or with PFT-μ. $n(AAVS1) = 3$, $n(CD4) = 6$, $n(PDCD1) = 6$, biological replicates, paired t test.

(B) Percentages of *AAVS1* modified NGS reads and CD4 and PD-1 protein levels of DMSO or PFT-α-treated activated CD4 T cells determined by flow cytometry. $n(AAVS1) = 3$, $n(CD4) = 6$, $n(PDCD1) = 7$, biological replicates, paired t test.

(C) Representative histograms of CFSE dilution patterns in *AAVS1*, *CD4*, and *PDCD1* KO T cells treated with PFT-μ/α.

(D) Quantification of fast-proliferating (CFSE-low) cells in *AAVS1*, *CD4*, and *PDCD1* KO T cells treated with PFT-μ/α. Cells were pre-gated on CD4- or PD-1-negative cells, respectively. Medians are indicated. Paired t test.

(E) Detected deletion sizes by amplicon NGS in non-activated, fast or slowly dividing CRISPR-Cas9-edited T cells with DMSO or PFT-μ. $n(AAVS1, CD4, PDCD1) = 3$, biological replicates. Data correspond to (C) and (D).

(F) Deletion sizes based on the activation and proliferation speed in CD4 T cells incubated with DMSO or PFT-α determined by amplicon NGS. Conditions with non-activated T cells and non-inhibitor-treated cells are the same as shown in Figure 2C. $n(AAVS1) = 3$, $n(CD4) = 3$, $n(PDCD1) = 4$, biological replicates. Data correspond to (C) and (D).

(G and H) NGS quantification of *AAVS1* (G) and *TP53* KO rates (H) in *AAVS1* and *TP53* double-edited T cells after PFT-μ/α treatment. Cells were pre-sorted on $CD4^-$ or PD-1-negative cells, respectively. Medians are indicated. Two-way ANOVA with Tukey's multiple comparison test.

(I and J) Amplicon NGS results of *AAVS1_CD4*, *AAVS1_PDCD1*, *TP53_CD4*, and *TP53_PDCD1*-edited T cells after the addition of PFT-μ/α. (G–J) $n(CD4) = 4$, $n(PDCD1) = 5$, biological replicates.

ns: not significant, $^*p < 0.05$, $^{***}p < 0.001$.

Next, we applied PFT-α to CD8 T cells during CRISPR editing. PFT-α treatment in *PDCD1* KO CD8 T cells reduced deletion sizes in cells with high and low cell division speeds while cell proliferation and KO efficiency were maintained (Figures S2I–S2N). The subset composition and cytokine profile of the control and PFT-α-treated cells were unaltered (Figures S2O and S2P). Overall, the deletion patterns at the *PDCD1* locus were similar between *PDCD1* KO CD4 and CD8 T cells with or without PFT-α with slightly higher mean deletion sizes in *PDCD1* KO CD4 T cells (Figures 3F and S2J; Table S2). CRISPR editing in the presence of PFT-α maintained the cytokine profiles and T cell subset compositions in both CD4 and CD8 KO T cells.

T cell subset-specific effects of PFT-α during CRISPR engineering

Understanding potential T cell subset-specific effects of PFT-α could inform future protocols for clinical T cell products as these subsets differ in their expansion, persistence, and differentiation potential.[37] Therefore, we assessed if TN, TEM, and TCM cells exhibit different sensitivities toward CRISPR engineering in the presence of PFT-α. We isolated the T cell subsets based on their CCR7/CD45RA expression pattern and performed PD-1 KOs as previously described (Figure S3). PD-1 protein levels were reduced in all conditions (Figures 4A and 4B). To exclude a bias due to different PD-1 expression levels in the subsets, KO efficiencies were independently confirmed on the DNA level. The KO rates in TN cells were reduced after PFT-α addition, while the other tested subsets were not affected (Figure 4C). We observed a reduction in cell divisions specifically in PFT-α-treated TEM cells and an increase in TCM cells (Figure 4D). After 1 week of culture, the T cell subset compositions of the cell cultures started with pure TN, TEM, and TCM cells were not significantly altered between PFT-α and DMSO conditions. We detected in all tested conditions a certain amount of CCR7+ CD45RA+ cells after KO and *in vitro* TCR stimulation. These cells with a TN-like surface marker composition have also been referred to as "TN-like" naive memory cells in similar contexts.[38] We therefore refer to these cells as TN-like cells hereafter (Figures 4E–4G). Overall, PFT-α does not interfere with the cellular differentiation programs of purified TN, TEM, and TCM cells (Figures 4E–4G; gating strategy after treatment: Figure S3). Finally, the CFSE-labeled cells were flow sorted based on the CFSE dilution pattern and subjected to indel analysis. The enrichment of large deletions in fast-dividing cells was more prominent in heavily dividing TN and TCM cells compared to the less proliferative TEM cells used as input cell material. However, PFT-α reduced the deletion sizes in all tested CD4 T cell populations (Figures 4H–4J; Table S2). Based on the cell donor's T cell subset composition, PFT-α can affect overall KO efficiencies and proliferation speed differently. But, importantly, PFT-α reduces the mutational burden independent of the nature of the subset while maintaining the cells' differentiation potential.

Impact of PFT-α treatment on CAR T cell engineering and function

Several phase 1 clinical trials pioneered CRISPR-engineered CAR T cells in the clinic to improve the clinical outcomes for various tumor entities.[1,2] Upon the first gene targets was the TCRα-encoding gene locus (*TRAC*), which is an attractive hub for both CRISPR KIs and gene KOs.[1,39] To test if PFT-α treatment could be beneficial for the genomic safety profile of these CAR - T cell products, CD8 T cells were pre-activated with ImmunoCult for 48 h, nucleofected with NT-, *AAVS1*-, or *TRAC*-targeting Cas9 RNPs, and treated with PFT-α or DMSO followed by retroviral transduction with a CD19-targeting CAR (Figure 5A). This stronger T cell activation protocol resulted in a higher cell proliferation rate and a higher frequency of large deletions compared to the post-activation protocol applied before (comparison of different T cell activation strategies: Figure S4). The *AAVS1* KO rates were reduced while *TRAC* KO rates were unaffected by inhibitor treatment (Figure 5A). PFT-α reduced again large deletions compared to control at both loci (Figures 5A and 5B; Table S2). To test the functionality of the CAR T cells, we challenged the cells with CD19-expressing Nalm6 ffluc-GFP tumor cells (firefly luciferase) in a co-culture assay with different T cell:tumor cell ratios. After 4 h, the IFNγ production was comparable in all conditions tested (Figure 5C). We did not detect differences in the tumor cell-killing capacities of PFT-α-treated CAR T cells after 24 h (Figure 5D). Next, we decided to challenge the cells in a preclinical humanized mouse model. Shortly, *TRAC* KO CD4 and CD8 CAR T cells were engineered as described before, and the deletion pattern with or without PFT-α treatment was confirmed by amplicon NGS (Figures 5E and 5F; Table S2). Nalm6 ffluc-GFP tumor cells were implanted into NSGS mice, and after 1 week, *TRAC* KO T cells engineered in the presence of DMSO or PFT-α or untransduced, unedited T cells (mock control) were injected into the mice (Figure 5E). The tumor progression was monitored via bioluminescence measurements and blood draws at day 6 and day 9 after injections (Figures 5G–5K). The number of CAR-positive T cells in the peripheral blood as well as the tumor cell numbers were unchanged between DMSO- and PFT-α-treated KO cells at day 6 (Figures 5G–5J). On day 9 after CAR T cell transfer, mice were sacrificed, and Nalm6 ffluc-GFP tumor burdens in the blood, spleen, and bone marrow were assessed. Tumor cells could still be detected in the bone marrow and their frequencies were comparable in both KO conditions (Figures 5G, 5H, 5J, and 5K). At day 9, no CAR-positive T cells could be detected anymore, independent of the KO condition (data not shown).

In summary, PFT-α reduced deletion sizes in *TRAC* KO CAR T cells without affecting transduction rates, IFNγ production, or killing capacities *in vitro* and *in vivo*.

PFT-α reduces the frequency of chromosomal aberrations and aneuploidy

CRISPR-induced chromosomal aberrations have been a major concern in the field.[10] For example, in T cell products with multiple simultaneous KOs, chromosomal translocations have been reported.[1] To assess the impact of TCR stimulation and PFT-α on larger deletions at the on-target site (>200 bp) as well as chromosomal translocations, we performed chromosomal aberrations analysis by single targeted linker-mediated PCR sequencing (CAST-seq), an NGS-based method to discover on-target gene deletions and chromosomal aberrations.[40] To induce chromosomal translocations, we simultaneously

Please cite this article in press as: Ursch et al., Modulation of TCR stimulation and pifithrin-α improves the genomic safety profile of CRISPR-engineered human T cells, Cell Reports Medicine (2024), https://doi.org/10.1016/j.xcrm.2024.101846

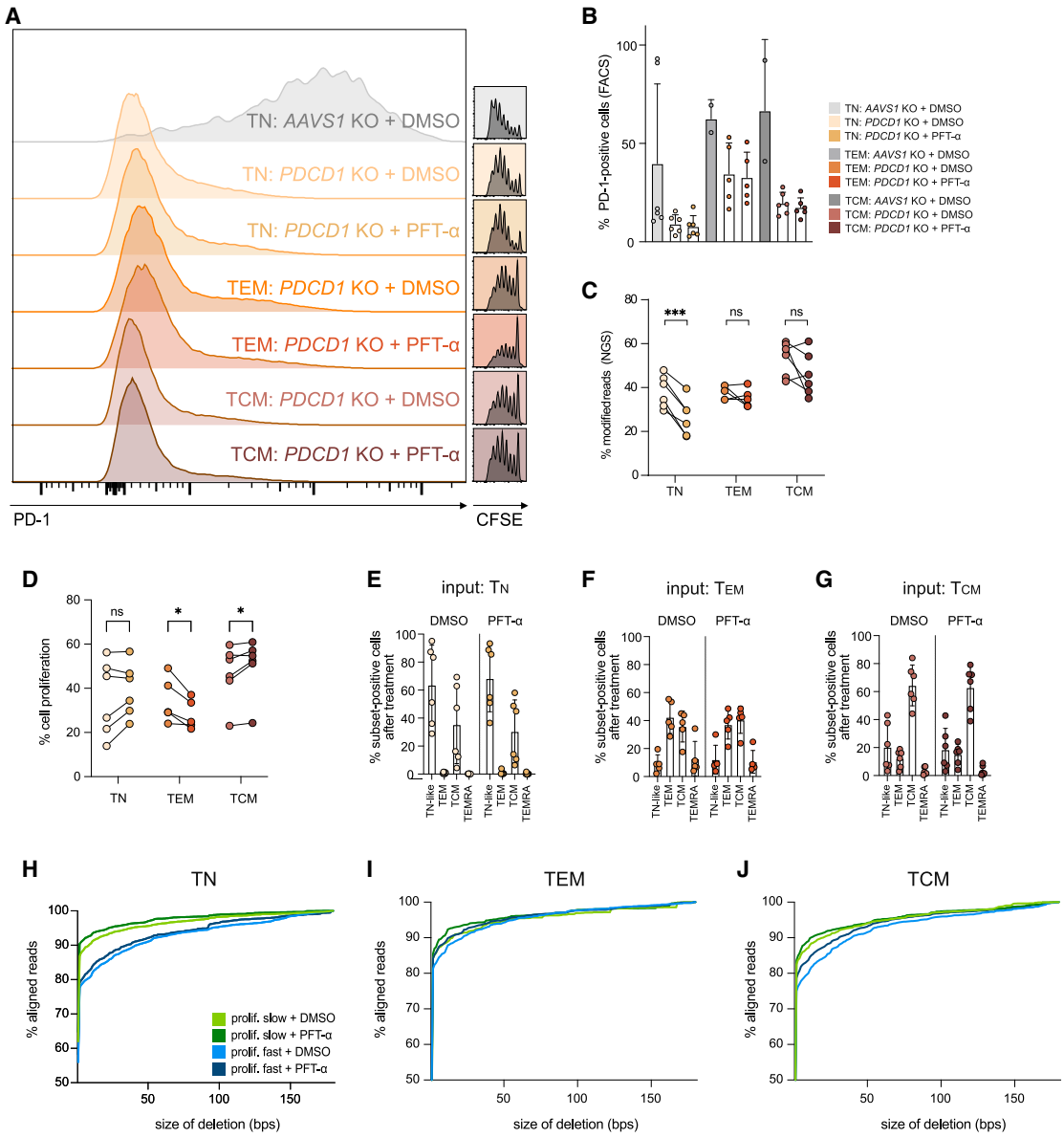

Figure 4. Impact of PFT-α on CD4 T cell subsets

TN, TEM, and TCM cells were flow purified, CFSE labeled, nucleofected with Cas9 RNPs, and treated with either DMSO or PFT-α.

(A) Representative example of PD-1 expression levels in different CD4 T cell subsets of one donor with either *AAVS1* or *PDCD1* KO. *PDCD1* KO T cells were treated with DMSO or PFT-α. The respective CFSE dilution pattern of each sample is depicted on the right.

(B) PD-1 expression levels in *AAVS1* KO and *PDCD1* KO TN, TEM, and TCM cells. *PDCD1* KO: n(TN) = 6, n(TEM) = 5, n(TCM) = 6; *AAVS1* KO: n(TN) = 6, n(TCM) = 2, n(TEM) = 2, biological replicates. Means with SD are shown.

(C) Percentage of modified *PDCD1* reads with DMSO or PFT-α treatment. Paired t test.

(D) Percentage of cell proliferation based on CD4-positive CFSE_low T cells in TN, TEM, and TCM cells with or without PFT-α treatment (gating: Figure S3). Paired t test.

(E–G) Subset compositions of input TN (E), TEM (F), and TCM (G) cells after KO, TCR stimulation, and DMSO or PFT-α treatment (gated on TN-like, TEM, TCM, and TEMRA; gating strategy: Figure S5). Two-way ANOVA with Šídák's multiple comparison test; no significant changes detected.

(H–J) Aligned reads of fast and slow proliferating T cells in TN (H), TEM (I), and TCM (J) cells with and without PFT-α treatment.

(E–J) n(TN) = 6, n(TEM) = 5, n(TCM) = 6, biological replicates.

ns: not significant, $^{*}p < 0.05$, $^{***}p < 0.001$.

Please cite this article in press as: Ursch et al., Modulation of TCR stimulation and pifithrin-α improves the genomic safety profile of CRISPR-engineered human T cells, Cell Reports Medicine (2024), https://doi.org/10.1016/j.xcrm.2024.101846

CellPress
OPEN ACCESS

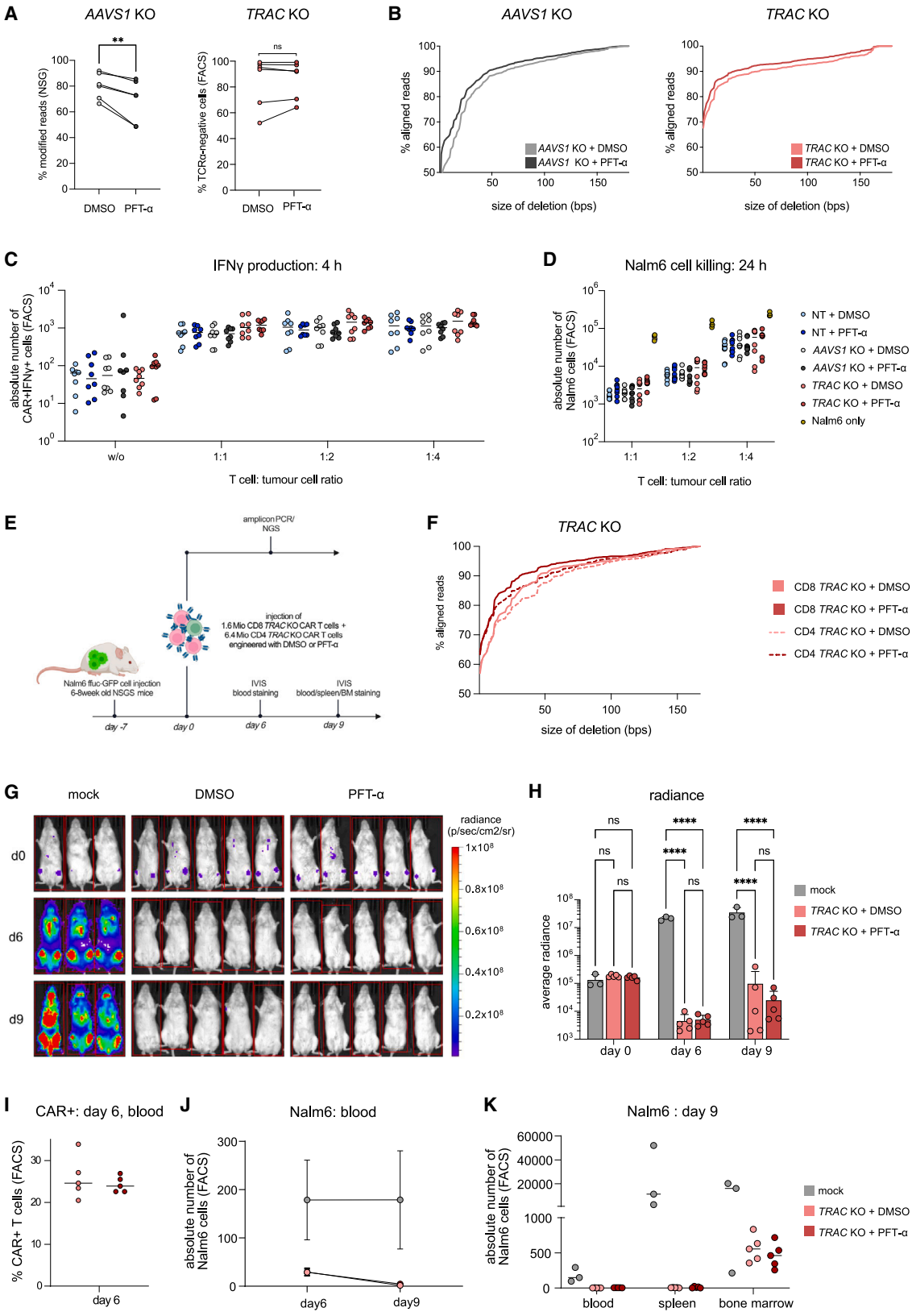

(legend on next page)

Please cite this article in press as: Ursch et al., Modulation of TCR stimulation and pifithrin-α improves the genomic safety profile of CRISPR-engineered human T cells, Cell Reports Medicine (2024), https://doi.org/10.1016/j.xcrm.2024.101846

targeted the *CD4* (chr12) and *PDCD1* (chr2) gene loci in activated and non-activated T cells and performed CAST-seq by analyzing the *CD4* site and employing the D-CAST-seq bioinformatic pipeline to take into account cleavage by two nucleases.[41] As expected, translocations between the *CD4* and *PDCD1* loci were detected in all samples by CAST-seq and droplet digital PCR (Figures 6A and S5C).

In order to look at on-target aberrations in more detail, the normalized read coverage in a region ± 5 kb around the *CD4* on-target site was plotted for each sample. While in the non-activated cells, the reads mostly stemmed from a narrow window around the cleavage site, large deletions, and inversions were readily detected in the activated cells, which were reduced in size and frequency in the PFT-α-treated samples (Figure 6B).

To quantify the number of large on-target deletions and inversions, the fraction of CAST-seq reads with a distance of more than 200 bp from the cleavage site was determined. We observed an increase in large on-target aberrations in activated cells, which was significantly reduced after PFT-α treatment (Figure 6C). In addition, when computing all deletions, we observed a significant decrease in the average deletion size in activated T cells when comparing PFT-α-treated to DMSO control samples (Figure 6D). Of particular interest, the frequency of translocations between the *CD4* and *PDCD1* loci was higher in the activated than in non-activated T cells but could be significantly reduced with PFT-α (Figure 6E). Consistent with these observations, CAST-seq coverage plots of the *PDCD1* locus confirmed that translocation junctions to the *CD4* locus clustered within 200 bp of the *PDCD1* target site in non-activated T cells, whereas they spread within a region of ± 3 kb in activated T cells (Figure S5A).

In PFT-α-treated, activated *CD4 PDCD1* double KO T cells, an off-target-mediated translocation was identified with the gene-coding region for *RABL6* (chr9) (Figure 6A). We observed similar levels of *RABL6* off-target mutations with our amplicon NGS pipeline in activated and non-activated T cells treated with DMSO or PFT-α (Figure S5B). It should be noted, however, that the signals for this off-target mutation were close to the limit of detection for both CAST-seq and NGS analysis. Overall, the induction of large deletions is strongly dependent on the activation status of the cells and PFT-α reduces the size and the frequency of these events.

Aneuploidy after CRISPR editing has not been recognized as a frequently occurring problem for a long time. Recent publications highlighted aneuploid human TCRα (gene: *TRAC*; chr14) KO T cells in frequencies of up to 20% after CRISPR editing, which can sustain extended periods of *in vitro* culture with potential risk for patients upon adoptive transfer.[10,11] Single-cell RNA sequencing (RNA-seq) analysis of Tsuchida et al. demonstrated that the T cell activation status is a major determent of this copy-number variation.[11] We applied single-cell Karyo-seq (scKaryo-seq) to assess the genomic integrity of individual cells directly by analyzing the genomic DNA and tested if PFT-α can reduce CRISPR-induced aneuploidy in *TRAC* KO T cells.[42,43] In non-activated, flow-sorted *TRAC* KO T cells, no aneuploidy induction at chr14 could be detected (Figures S6A and S6B, cell numbers indicated). Next, CD8 T cells were pre-activated for 48 h with anti-CD3/28-coated beads in a 1:1 bead:cell ratio before editing the *TRAC* locus similar to the protocol used by Tsuchida et al. and in clinical studies (comparison of different T cell activation strategies, Figure S4).[2,11] Also, in this case, the strong pre-activation resulted in higher T cell proliferation and large deletions in a higher frequency. We also tested the addition of IL-7 and IL-15 to the pre-activated cells as applied by Tsuchida et al. and detected similar deletion patterns based on amplicon NGS (Figure S4C).[11] Editing of the TCRα chain induced haploidy in 13% of the cells, which is in line with previous studies.[10,11] However, adding PFT-α after Cas9 RNP nucleofection reduced the number of chr14 haploid cells significantly to 3% while maintaining global genomic integrity (Figures 5F, S6C, and S6D).

TCR stimulation is a major driver of large-scale chromosomal aberrations, translocations and aneuploidy. Adjusting T cell activation and the addition of PFT-α can counteract these events, thereby increasing the genomic integrity of CRISPR-engineered human T cells.

Figure 5. Functionality of CAR T cells engineered in the presence of PFT-α

(A) CD8 T cells were activated, nucleofected with NT-, *AAVS1*-, or *TRAC*-targeting Cas9 RNPs, transduced 48 h later with αCD19-CAR retrovirus, and treated with DMSO or PFT-α. KO rates of *AAVS1* and *TRAC* KO CAR T cells with or without PFT-α treatment. Paired t test.

(B) Deletion sizes in *AAVS1* and *TRAC* KO cells with DMSO or PFT-α.

(A and B) $n = 6$, biological replicates.

(C) IFNγ-positive CAR T cells after 4 h in Nalm6 ffluc-GFP killing assay in different CAR T cell:tumor cell ratios.

(D) Nalm6 ffluc-GFP cell count after 24 h co-culture with CAR T cells.

(C and D) Killing assays were performed in technical duplicates. Means are indicated. $n = 4$, biological replicates. Results of DMSO and PFT-α conditions were normalized for differences in transduction rates. two-way ANOVA (mixed-effects model) with Tukey's multiple comparison test; no significant changes were detected between the respective DMSO and PFT-α groups.

(E) Outline of *TRAC* KO CAR T cell challenge in Nalm6 ffluc-GFP tumor model in NSGS mice.

(F) Deletion sizes in *TRAC* KO CAR CD4 and CD8 T cells engineered in the presence of DMSO or PFT-α. $n = 1$.

(G) Bioluminescence pictures of Nalm6 ffluc-GFP tumor burden at day 0, 6, and 9 of mock-treated mice and mice treated with *TRAC* KO CAR T cells with or without PFT-α.

(H) Quantification of bioluminescence signal of mice shown in (G). Unspecific head signals were excluded from the analysis. Two-way ANOVA, mean with SD is shown.

(I) Frequency of CAR-positive T cells in the peripheral blood at day 6. Median is depicted.

(J) Nalm6 ffluc-GFP tumor cell counts in the peripheral blood at day 6 and 9. Mean with SD.

(K) Nalm6 ffluc-GFP tumor cell counts in blood, spleen, and bone marrow at day 9 after CAR T cell injection. Median is shown.

(F–K): n(mock) = 3, n(*TRAC* KO + DMSO, *TRAC* KO + PFT-α) = 5.

ns: not significant, $^{**}p < 0.01$, $^{****}p < 0.0001$.

Please cite this article in press as: Ursch et al., Modulation of TCR stimulation and pifithrin-α improves the genomic safety profile of CRISPR-engineered human T cells, Cell Reports Medicine (2024), https://doi.org/10.1016/j.xcrm.2024.101846

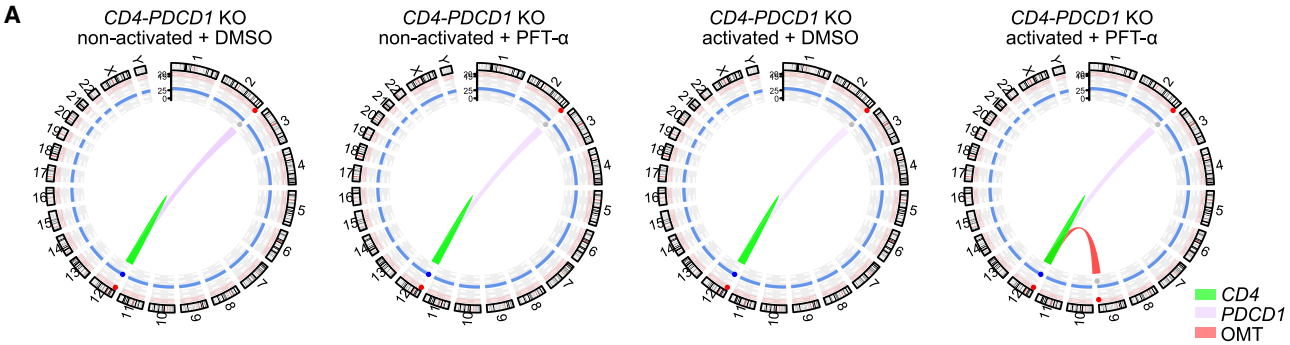

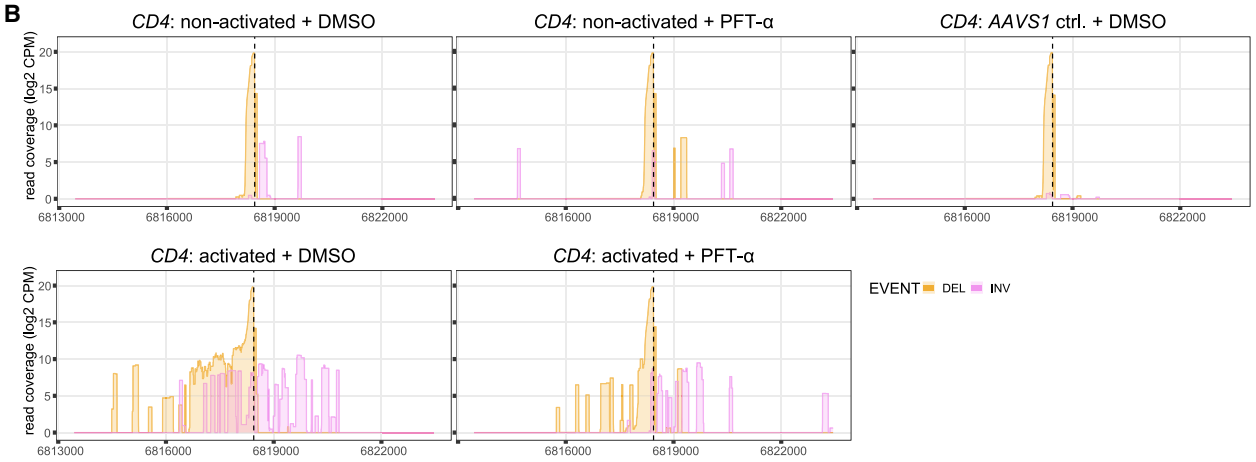

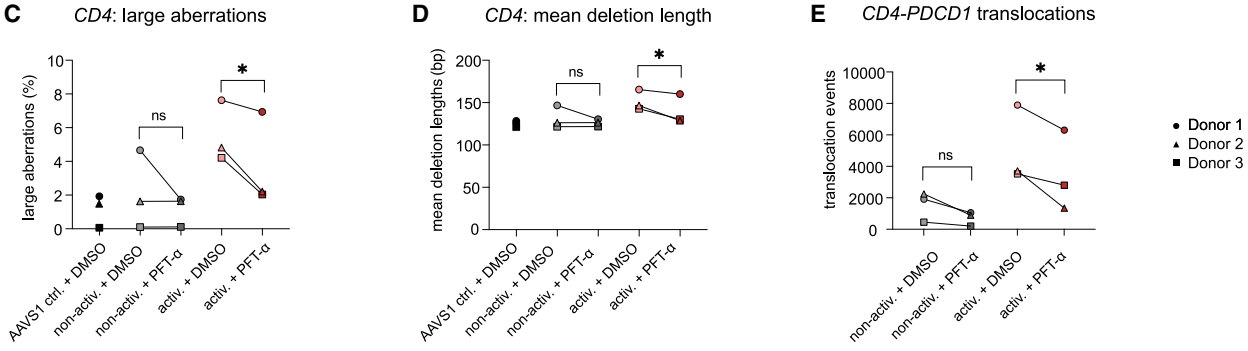

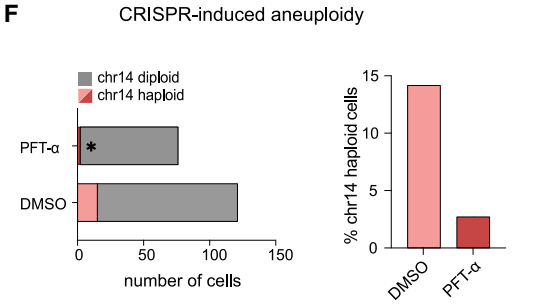

(legend on next page)

Please cite this article in press as: Ursch et al., Modulation of TCR stimulation and pifithrin-α improves the genomic safety profile of CRISPR-engineered human T cells, Cell Reports Medicine (2024), https://doi.org/10.1016/j.xcrm.2024.101846

DISCUSSION

There is increasing evidence that CRISPR-Cas9 engineering can result in significant large DNA deletions, chromosomal rearrangements, and even aneuploidy that potentially negatively affect gene function in various cell types.[7–11,28] However, CRISPR-engineered CAR T cells are now already applied in the clinic. This underscores the urgent need to understand the cell type-specific driving forces of CRISPR-induced chromosomal aberrations.[1–3]

Our data show that non-activated T cells carry a lower risk for large deletions and chromosomal translocations during CRISPR-Cas9 editing compared to activated T cells. These results are in line with very recent studies describing similar observations that T cell activation or cell proliferation can be risk factors for such events.[11,28] In addition to the similar basic observations, we demonstrate with our study the influence of TCR stimulation—the time point of TCR stimulation prior to editing as well as the strength of TCR activation—on a wide range of chromosomal aberrations in human T cells. One disadvantage of applying non-activated T cells for CRISPR-Cas9 engineering is the reduced number of KO cells generated, which may not be sufficient for adoptive T cell therapies. T cell stimulation after the completion of DNA repair can be an alternative strategy to reach adequate KO cell numbers. However, gene loci not expressed in resting T cells are less accessible to CRISPR engineering due to heterochromatin formation.[44,45] Besides that, CRISPR-Cas9 KI protocols for human T cells depend on strong TCR stimulation prior to Cas9 RNP nucleofection, although the addition of HDR templates can counteract large deletions to some extent.[17,18]

Alternatively, we observed a reduction of chromosomal aberrations including CRISPR-induced aneuploidy by adding the small-molecule PFT-α directly after nucleofection. Importantly, *in vitro* proinflammatory cytokine production and T cell subset composition were unaffected in T cells engineered in the presence of PFT-α. However, we detected also subset-specific effects of PFT-α. PFT-α reduced the KO efficiency in TN cells. Cell proliferation was decreased in TEM cells while we observed an increase in TCM cell divisions, hinting toward subset-specific regulation of cell proliferation, which has been described before.[46] *In vitro* tumor-killing capacities of CRISPR-engineered CAR T cells edited in the presence of DMSO or PFT-α were unaltered. Also, in a preclinical tumor mouse model, cancer cell clearance was as efficient as with control CAR T cells over a time period of 9 days. A prerequisite to potentially apply PFT-α in clinical T cell products is the availability of GMP-grade PFT-α and a thorough genotoxic safety assessment of the cell product before adoptive T cell transfer.

PFT-α has been widely described as a p53 inhibitor. However, in our experimental setup, PFT-α functioned independently of p53. A previous study identified PFT-α as an inhibitor of DNA damage-induced apoptosis by combined interference with caspase-3, caspase-9, and cyclin D1 function.[34] In our assays, we could not detect increased KO cell yields with PFT-α, which would be indicative of improved KO cell survival and inhibition of apoptosis induction. Interference with cyclin D1, a key regulator of the G1-S cell cycle checkpoint, can potentially slow down cell cycle progression temporarily, thereby providing extended time for DNA repair.[47] Other reports identified the aryl hydrocarbon receptor and glucocorticoid receptors as additional PFT-α targets, which can also interfere with cell proliferation, but also with multiple other cell functions.[35,48–50] Interestingly, in other cell types, extended PFT-α inhibitor treatment has been reported to increase deletion sizes during CRISPR editing.[28] Further studies are therefore needed to systematically characterize PFT-α's targets and its complex—potentially combinatorial—effects, in a cell type- and context-specific manner for instance by RNA-seq analysis of inhibitor-treated KO cells or by global, unbiased approaches such as thermal proteome profiling, click chemistry approaches, or metabolic fingerprinting.[51–53]

Several measures can reduce the risk of large gene deletions in human T cells such as selecting optimized gRNAs or switching to alternative nucleases.[12,13,15,16] We propose here optimized T cell activation protocols and the addition of PFT-α as easily implementable alternative strategies to reduce large deletions, translocations, and aneuploidy for clinical T cell products in the future.

Limitations of the study

In our study, we analyzed the deletion pattern at five genetic loci. Potentially, the gRNA sequence itself can impact not only the frequency of small off-target mutations but also chromosomal aberrations.[54] To determine the interconnection between gRNA, the targeted chromatin region, and the frequency of chromosomal aberrations, more gRNAs with different off- and on-target efficiencies targeting the same gene need to be tested. CAST-seq analysis revealed one off-target mutation in activated double-edited T cells. The here applied methodologies are not

Figure 6. Impact of PFT-α on CRISPR-induced chromosomal aberrations and aneuploidy

(A) Chromosomal rearrangements. Circos plot visualization of chromosomal aberrations at the *CD4* target locus in activated and non-activated T cells treated with or without PFT-α as detected by CAST-Seq. *CD4*: Chromosomal aberrations at on-target site. *PDCD1*: Chromosomal translocations to *PDCD1* target locus. OMT: off-target-mediated translocation to *RABL6* locus.

(B) Representative example of CAST-seq read coverage plots of ± 5 kb around the *CD4* on-target site (donor 2 is depicted). The x axis indicates the chromosomal coordinates, the y axis the log2 read count per million (CPM), and the dotted line the cleavage site. Deletions (DEL) are shown in orange, inversions (INV) in purple.

(C) Percentage of large chromosomal aberrations. Fraction of CAST-seq reads with a distance of more than 200 bp from the cleavage site within a ± 5 kb window around the cleavage site.

(D) Mean deletion lengths at the *CD4* locus.

(E) Quantification of chromosomal translocations to *PDCD1* locus. Translocation reads were normalized to absolute read numbers. (C–E) One-tailed paired t test. (A–E) $n = 3$, biological replicates.

(F) Chromosomal loss. Number of *TRAC* KO cells treated with or without PFT-α with CRISPR-induced chromosome 14 (chr14) haploidy or diploidy analyzed by scKaryo-seq (left). Percentage of chr14 haploid cells (right). Combined analysis of cells of two donors. Fisher's exact test.

ns: not significant, $^*p < 0.05$.

optimized for detecting low-frequency off-target mutations, and future studies implementing, for example, DISCOVER-seq could be informative.[55] We monitored the functionality of CAR T cells engineered in the presence of PFT-α over 9 days in a Nalm6 tumor model. Future studies are needed to assess different cell parameters after extended periods of time, potentially also in syngeneic tumor mouse models.

RESOURCE AVAILABILITY

Lead contact

Further information and requests for resources and reagents should be directed to and will be fulfilled by the lead contact, Kathrin Schumann (kathrin.schumann@tum.de).

Materials availability

This study did not generate new unique reagents.

Data and code availability

- Amplicon NGS and CAST-seq datasets are publicly available on the GEO database (GSE249934 and GSE249194). scKaryo-seq NGS data are available upon request at the EGA database (EGA: EGAS50000000656).
- This study did not generate original code.
- Any additional information required to reanalyze the data reported in this work paper is available from the lead contact upon request.

ACKNOWLEDGMENTS

We thank the members of the Schumann laboratory for helpful suggestions and technical assistance. We especially thank Immanuel Andrä, Katharina Hofmann, Tanja Roßmann-Bloeck, and Corinne Angerpointner for cell sorting assistance and Monika Hammel for NGS support. The authors would like to thank Single-Cell Core of the Oncode Institute, Utrecht, the Netherlands, for performing the single-cell sample preparation and Barbason Biotech for performing scKaryo-seq analysis. We kindly thank Stanley Riddell for Nalm6 ffluc-GFP cell line. We are thankful to Raquel Mejias Luque for providing critical feedback on this study. We acknowledge support by the Core Facility "CyTUM MIH" in cell sorting (DFG instrument funding within project no. 659391 and 659389). L.T.U. and K.S. (2020_EKEA.192) received support from the Else Kröner-Fresenius-Stiftung. This work was funded by the Deutsche Forschungsgemeinschaft (DFG, German Research Foundation) grants SFB1054/3 – 210592381 (project B09 [D.H.B.] and B16 [K.S.]), SFB-TRR 338/1 2021 – 452881907 (project A01 [D.H.B.], C04 [K.S.], and Z03 [F.J.T.]), and SFB-TRR 355/1 2022 – 490846870 (project A07) to K.S. and grant CA 311/4 (project FANEDIT) to T.C. We also acknowledge funding from the German Federal Ministry of Education and Research (BMBF) within the Medical Informatics Funding Scheme (projects PM4Onco–FKZ 01ZZ2322A and EkoEstMed–FKZ 01ZZ2015) to M.B. and G.A.

AUTHOR CONTRIBUTIONS

L.T.U. and K.S. designed research; L.T.U., J.S.M., J.R., J.K., B.E.B., and S.K. performed research; J.K., G.A., M.B., and T.C. designed, performed, and analyzed CAST-seq data; L.W., J.S.M., B.E.B., S.K., and D.H.B. designed, performed, and analyzed *in vivo* CAR T cell experiment; G.M., M.J.-M., and F.J.T. provided statistical advice; L.T.U., J.S.M., J.R., B.E.B., S.K., and K.S. analyzed data; and K.S. wrote the manuscript with the support of all authors.

DECLARATION OF INTERESTS

The authors declare no competing interests.

STAR★METHODS

Detailed methods are provided in the online version of this paper and include the following:

- KEY RESOURCES TABLE
- EXPERIMENTAL MODEL AND STUDY PARTICIPANT ANALYSIS
  - Mouse model
  - Primary human T cells
- METHOD DETAILS
  - Isolation and culture of primary human T cells
  - Cas9 RNP assembly and nucleofection
  - CFSE T cell proliferation assay
  - Flow cytometry analysis
  - Flow cytometry cell sorting and DNA extraction
  - Retrovirus production
  - CAR T cell engineering
  - *In vitro* killing assay
  - Nalm6 *in vivo* tumor model
  - CAST-seq analysis
  - ddPCR
  - scKaryo-seq analysis
  - Amplicon NGS
- QUANTIFICATION AND STATISTICAL ANALYSIS

SUPPLEMENTAL INFORMATION

Supplemental information can be found online at https://doi.org/10.1016/j.xcrm.2024.101846.

Received: February 5, 2024
Revised: June 24, 2024
Accepted: November 11, 2024
Published: December 4, 2024

REFERENCES

1. Stadtmauer, E.A., Fraietta, J.A., Davis, M.M., Cohen, A.D., Weber, K.L., Lancaster, E., Mangan, P.A., Kulikovskaya, I., Gupta, M., Chen, F., et al. (2020). CRISPR-engineered T cells in patients with refractory cancer. Science *367*, eaba7365. https://doi.org/10.1126/science.aba7365.
2. Foy, S.P., Jacoby, K., Bota, D.A., Hunter, T., Pan, Z., Stawiski, E., Ma, Y., Lu, W., Peng, S., Wang, C.L., et al. (2023). Non-viral precision T cell receptor replacement for personalized cell therapy. Nature *615*, 687–696. https://doi.org/10.1038/s41586-022-05531-1.
3. Ottaviano, G., Georgiadis, C., Gkazi, S.A., Syed, F., Zhan, H., Etuk, A., Preece, R., Chu, J., Kubat, A., Adams, S., et al. (2022). Phase 1 clinical trial of CRISPR-engineered CAR19 universal T cells for treatment of children with refractory B cell leukemia. Sci. Transl. Med. *14*, eabq3010. https://doi.org/10.1126/scitranslmed.abq3010.
4. Freen-van Heeren, J.J. (2022). Closing the Door with CRISPR: Genome Editing of CCR5 and CXCR4 as a Potential Curative Solution for HIV. BioTech (Basel) *11*, 25. https://doi.org/10.3390/biotech11030025.
5. Rupp, L.J., Schumann, K., Roybal, K.T., Gate, R.E., Ye, C.J., Lim, W.A., and Marson, A. (2017). CRISPR/Cas9-mediated PD-1 disruption enhances anti-tumor efficacy of human chimeric antigen receptor T cells. Sci. Rep. *7*, 737. https://doi.org/10.1038/s41598-017-00462-8.
6. Ren, J., Liu, X., Fang, C., Jiang, S., June, C.H., and Zhao, Y. (2017). Multiplex Genome Editing to Generate Universal CAR T Cells Resistant to PD1 Inhibition. Clin. Cancer Res. *23*, 2255–2266. https://doi.org/10.1158/1078-0432.CCR-16-1300.
7. Schumann, K., Lin, S., Boyer, E., Simeonov, D.R., Subramaniam, M., Gate, R.E., Haliburton, G.E., Ye, C.J., Bluestone, J.A., Doudna, J.A., and Marson, A. (2015). Generation of knock-in primary human T cells using Cas9

ribonucleoproteins. Proc. Natl. Acad. Sci. USA *112*, 10437–10442. https://doi.org/10.1073/pnas.1512503112.

8. Kosicki, M., Rajan, S.S., Lorenzetti, F.C., Wandall, H.H., Narimatsu, Y., Metzakopian, E., and Bennett, E.P. (2017). Dynamics of Indel Profiles Induced by Various CRISPR/Cas9 Delivery Methods. Prog. Mol. Biol. Transl. Sci. *152*, 49–67. https://doi.org/10.1016/bs.pmbts.2017.09.003.
9. Cullot, G., Boutin, J., Toutain, J., Prat, F., Pennamen, P., Rooryck, C., Teichmann, M., Rousseau, E., Lamrissi-Garcia, I., Guyonnet-Duperat, V., et al. (2019). CRISPR-Cas9 genome editing induces megabase-scale chromosomal truncations. Nat. Commun. *10*, 1136. https://doi.org/10.1038/s41467-019-09006-2.
10. Nahmad, A.D., Reuveni, E., Goldschmidt, E., Tenne, T., Liberman, M., Horovitz-Fried, M., Khosravi, R., Kobo, H., Reinstein, E., Madi, A., et al. (2022). Frequent aneuploidy in primary human T cells after CRISPR-Cas9 cleavage. Nat. Biotechnol. *40*, 1807–1813. https://doi.org/10.1038/s41587-022-01377-0.
11. Tsuchida, C.A., Brandes, N., Bueno, R., Trinidad, M., Mazumder, T., Yu, B., Hwang, B., Chang, C., Liu, J., Sun, Y., et al. (2023). Mitigation of chromosome loss in clinical CRISPR-Cas9-engineered T cells. Cell *186*, 4567–4582.e20. https://doi.org/10.1016/j.cell.2023.08.041.
12. Chakrabarti, A.M., Henser-Brownhill, T., Monserrat, J., Poetsch, A.R., Luscombe, N.M., and Scaffidi, P. (2019). Target-Specific Precision of CRISPR-Mediated Genome Editing. Mol. Cell *73*, 699–713.e6. https://doi.org/10.1016/j.molcel.2018.11.031.
13. Leenay, R.T., Vento, J.M., Shah, M., Martino, M.E., Leulier, F., and Beisel, C.L. (2019). Genome Editing with CRISPR-Cas9 in Lactobacillus plantarum Revealed That Editing Outcomes Can Vary Across Strains and Between Methods. Biotechnol. J. *14*, e1700583. https://doi.org/10.1002/biot.201700583.
14. Allen, F., Crepaldi, L., Alsinet, C., Strong, A.J., Kleshchevnikov, V., De Angeli, P., Páleníková, P., Khodak, A., Kiselev, V., Kosicki, M., et al. (2018). Predicting the mutations generated by repair of Cas9-induced double-strand breaks. Nat. Biotechnol. https://doi.org/10.1038/nbt.4317.
15. Komor, A.C., Kim, Y.B., Packer, M.S., Zuris, J.A., and Liu, D.R. (2016). Programmable editing of a target base in genomic DNA without double-stranded DNA cleavage. Nature *533*, 420–424. https://doi.org/10.1038/nature17946.
16. Petri, K., Zhang, W., Ma, J., Schmidts, A., Lee, H., Horng, J.E., Kim, D.Y., Kurt, I.C., Clement, K., Hsu, J.Y., et al. (2022). CRISPR prime editing with ribonucleoprotein complexes in zebrafish and primary human cells. Nat. Biotechnol. *40*, 189–193. https://doi.org/10.1038/s41587-021-00901-y.
17. Roth, T.L., Puig-Saus, C., Yu, R., Shifrut, E., Carnevale, J., Li, P.J., Hiatt, J., Saco, J., Krystofinski, P., Li, H., et al. (2018). Reprogramming human T cell function and specificity with non-viral genome targeting. Nature *559*, 405–409. https://doi.org/10.1038/s41586-018-0326-5.
18. Wen, W., Quan, Z.J., Li, S.A., Yang, Z.X., Fu, Y.W., Zhang, F., Li, G.H., Zhao, M., Yin, M.D., Xu, J., et al. (2021). Effective control of large deletions after double-strand breaks by homology-directed repair and dsODN insertion. Genome Biol. *22*, 236. https://doi.org/10.1186/s13059-021-02462-4.
19. Park, S.H., Cao, M., Pan, Y., Davis, T.H., Saxena, L., Deshmukh, H., Fu, Y., Treangen, T., Sheehan, V.A., and Bao, G. (2022). Comprehensive analysis and accurate quantification of unintended large gene modifications induced by CRISPR-Cas9 gene editing. Sci. Adv. *8*, eabo7676. https://doi.org/10.1126/sciadv.abo7676.
20. Schimmel, J., Muñoz-Subirana, N., Kool, H., van Schendel, R., van der Vlies, S., Kamp, J.A., de Vrij, F.M.S., Kushner, S.A., Smith, G.C.M., Boulton, S.J., and Tijsterman, M. (2023). Modulating mutational outcomes and improving precise gene editing at CRISPR-Cas9-induced breaks by chemical inhibition of end-joining pathways. Cell Rep. *42*, 112019. https://doi.org/10.1016/j.celrep.2023.112019.
21. Hu, Q., Xie, Y., Ge, Y., Nie, X., Tao, J., and Zhao, Y. (2018). Resting T cells are hypersensitive to DNA damage due to defective DNA repair pathway. Cell Death Dis. *9*, 662. https://doi.org/10.1038/s41419-018-0649-z.
22. McNally, J.P., Millen, S.H., Chaturvedi, V., Lakes, N., Terrell, C.E., Elfers, E.E., Carroll, K.R., Hogan, S.P., Andreassen, P.R., Kanter, J., et al. (2017). Manipulating DNA damage-response signaling for the treatment of immune-mediated diseases. Proc. Natl. Acad. Sci. USA *114*, E4782–E4791. https://doi.org/10.1073/pnas.1703683114.
23. Ihry, R.J., Worringer, K.A., Salick, M.R., Frias, E., Ho, D., Theriault, K., Kommineni, S., Chen, J., Sondey, M., Ye, C., et al. (2018). p53 inhibits CRISPR-Cas9 engineering in human pluripotent stem cells. Nat. Med. *24*, 939–946. https://doi.org/10.1038/s41591-018-0050-6.
24. Haapaniemi, E., Botla, S., Persson, J., Schmierer, B., and Taipale, J. (2018). CRISPR-Cas9 genome editing induces a p53-mediated DNA damage response. Nat. Med. *24*, 927–930. https://doi.org/10.1038/s41591-018-0049-z.
25. Watanabe, M., Moon, K.D., Vacchio, M.S., Hathcock, K.S., and Hodes, R.J. (2014). Downmodulation of tumor suppressor p53 by T cell receptor signaling is critical for antigen-specific CD4(+) T cell responses. Immunity *40*, 681–691. https://doi.org/10.1016/j.immuni.2014.04.006.
26. Hendel, A., Bak, R.O., Clark, J.T., Kennedy, A.B., Ryan, D.E., Roy, S., Steinfeld, I., Lunstad, B.D., Kaiser, R.J., Wilkens, A.B., et al. (2015). Chemically modified guide RNAs enhance CRISPR-Cas genome editing in human primary cells. Nat. Biotechnol. *33*, 985–989. https://doi.org/10.1038/nbt.3290.
27. Hafner, A., Bulyk, M.L., Jambhekar, A., and Lahav, G. (2019). The multiple mechanisms that regulate p53 activity and cell fate. Nat. Rev. Mol. Cell Biol. *20*, 199–210. https://doi.org/10.1038/s41580-019-0110-x.
28. Cullot, G., Boutin, J., Fayet, S., Prat, F., Rosier, J., Cappellen, D., Lamrissi, I., Pennamen, P., Bouron, J., Amintas, S., et al. (2023). Cell cycle arrest and p53 prevent ON-target megabase-scale rearrangements induced by CRISPR-Cas9. Nat. Commun. *14*, 4072. https://doi.org/10.1038/s41467-023-39632-w.
29. Komarov, P.G., Komarova, E.A., Kondratov, R.V., Christov-Tselkov, K., Coon, J.S., Chernov, M.V., and Gudkov, A.V. (1999). A chemical inhibitor of p53 that protects mice from the side effects of cancer therapy. Science *285*, 1733–1737. https://doi.org/10.1126/science.285.5434.1733.
30. Fraser, M., Chan, S.L., Chan, S.S.L., Fiscus, R.R., and Tsang, B.K. (2006). Regulation of p53 and suppression of apoptosis by the soluble guanylyl cyclase/cGMP pathway in human ovarian cancer cells. Oncogene *25*, 2203–2212. https://doi.org/10.1038/sj.onc.1209251.
31. Walton, M.I., Wilson, S.C., Hardcastle, I.R., Mirza, A.R., and Workman, P. (2005). An evaluation of the ability of pifithrin-alpha and -beta to inhibit p53 function in two wild-type p53 human tumor cell lines. Mol. Cancer Therapeut. *4*, 1369–1377. https://doi.org/10.1158/1535-7163.MCT-04-0341.
32. Zhu, J., Singh, M., Selivanova, G., and Peuget, S. (2020). Pifithrin-alpha alters p53 post-translational modifications pattern and differentially inhibits p53 target genes. Sci. Rep. *10*, 1049. https://doi.org/10.1038/s41598-020-58051-1.
33. Strom, E., Sathe, S., Komarov, P.G., Chernova, O.B., Pavlovska, I., Shyshynova, I., Bosykh, D.A., Burdelya, L.G., Macklis, R.M., Skaliter, R., et al. (2006). Small-molecule inhibitor of p53 binding to mitochondria protects mice from gamma radiation. Nat. Chem. Biol. *2*, 474–479. https://doi.org/10.1038/nchembio809.
34. Sohn, D., Graupner, V., Neise, D., Essmann, F., Schulze-Osthoff, K., and Jänicke, R.U. (2009). Pifithrin-alpha protects against DNA damage-induced apoptosis downstream of mitochondria independent of p53. Cell Death Differ. *16*, 869–878. https://doi.org/10.1038/cdd.2009.17.
35. Hoagland, M.S., Hoagland, E.M., and Swanson, H.I. (2005). The p53 inhibitor pifithrin-alpha is a potent agonist of the aryl hydrocarbon receptor. J. Pharmacol. Exp. Therapeut. *314*, 603–610. https://doi.org/10.1124/jpet.105.084186.
36. Jiang, L., Ingelshed, K., Shen, Y., Boddul, S.V., Iyer, V.S., Kasza, Z., Sedimbi, S., Lane, D.P., and Wermeling, F. (2022). CRISPR/Cas9-Induced DNA Damage Enriches for Mutations in a p53-Linked Interactome: Implications for CRISPR-Based Therapies. Cancer Res. *82*, 36–45. https://doi.org/10.1158/0008-5472.CAN-21-1692.

37. Busch, D.H., Fräßle, S.P., Sommermeyer, D., Buchholz, V.R., and Riddell, S.R. (2016). Role of memory T cell subsets for adoptive immunotherapy. Semin. Immunol. *28*, 28–34. https://doi.org/10.1016/j.smim.2016.02.001.

38. Frumento, G., Verma, K., Croft, W., White, A., Zuo, J., Nagy, Z., Kissane, S., Anderson, G., Moss, P., and Chen, F.E. (2020). Homeostatic Cytokines Drive Epigenetic Reprogramming of Activated T Cells into a "Naive-Memory" Phenotype. iScience *23*, 100989. https://doi.org/10.1016/j.isci.2020.100989.

39. Roth, T.L., Puig-Saus, C., Yu, R., Shifrut, E., Carnevale, J., Li, P.J., Hiatt, J., Saco, J., Krystofinski, P., Li, H., et al. (2018). Reprogramming human T cell function and specificity with non-viral genome targeting. Nature *559*, 405–409.

40. Turchiano, G., Andrieux, G., Klermund, J., Blattner, G., Pennucci, V., El Gaz, M., Monaco, G., Poddar, S., Mussolino, C., Cornu, T.I., et al. (2021). Quantitative evaluation of chromosomal rearrangements in gene-edited human stem cells by CAST-Seq. Cell Stem Cell *28*, 1136–1147.e5. https://doi.org/10.1016/j.stem.2021.02.002.

41. Klermund, J., Rhiel, M., Kocher, T., Chmielewski, K.O., Bischof, J., Andrieux, G., El Gaz, M., Hainzl, S., Boerries, M., Cornu, T.I., et al. (2024). On- and off-target effects of paired CRISPR-Cas nickase in primary human cells. Mol. Ther. *32*, 1298–1310. https://doi.org/10.1016/j.ymthe.2024.03.006.

42. Bolhaqueiro, A.C.F., Ponsioen, B., Bakker, B., Klaasen, S.J., Kucukkose, E., van Jaarsveld, R.H., Vivié, J., Verlaan-Klink, I., Hami, N., Spierings, D.C.J., et al. (2019). Ongoing chromosomal instability and karyotype evolution in human colorectal cancer organoids. Nat. Genet. *51*, 824–834. https://doi.org/10.1038/s41588-019-0399-6.

43. Bakker, B., Taudt, A., Belderbos, M.E., Porubsky, D., Spierings, D.C.J., de Jong, T.V., Halsema, N., Kazemier, H.G., Hoekstra-Wakker, K., Bradley, A., et al. (2016). Single-cell sequencing reveals karyotype heterogeneity in murine and human malignancies. Genome Biol. *17*, 115. https://doi.org/10.1186/s13059-016-0971-7.

44. Isaac, R.S., Jiang, F., Doudna, J.A., Lim, W.A., Narlikar, G.J., and Almeida, R. (2016). Nucleosome breathing and remodeling constrain CRISPR-Cas9 function. Elife *5*, e13450. https://doi.org/10.7554/eLife.13450.

45. Gemberling, M.P., Siklenka, K., Rodriguez, E., Tonn-Eisinger, K.R., Barrera, A., Liu, F., Kantor, A., Li, L., Cigliola, V., Hazlett, M.F., et al. (2021). Transgenic mice for in vivo epigenome editing with CRISPR-based systems. Nat. Methods *18*, 965–974. https://doi.org/10.1038/s41592-021-01207-2.

46. Kretschmer, L., Flossdorf, M., Mir, J., Cho, Y.L., Plambeck, M., Treise, I., Toska, A., Heinzel, S., Schiemann, M., Busch, D.H., and Buchholz, V.R. (2020). Differential expansion of T central memory precursor and effector subsets is regulated by division speed. Nat. Commun. *11*, 113. https://doi.org/10.1038/s41467-019-13788-w.

47. Pagano, M., Theodoras, A.M., Tam, S.W., and Draetta, G.F. (1994). Cyclin D1-mediated inhibition of repair and replicative DNA synthesis in human fibroblasts. Genes Dev. *8*, 1627–1639. https://doi.org/10.1101/gad.8.14.1627.

48. Komarova, E.A., Neznanov, N., Komarov, P.G., Chernov, M.V., Wang, K., and Gudkov, A.V. (2003). p53 inhibitor pifithrin alpha can suppress heat shock and glucocorticoid signaling pathways. J. Biol. Chem. *278*, 15465–15468. https://doi.org/10.1074/jbc.C300011200.

49. Clarisse, D., Offner, F., and De Bosscher, K. (2020). Latest perspectives on glucocorticoid-induced apoptosis and resistance in lymphoid malignancies. Biochim. Biophys. Acta Rev. Canc *1874*, 188430. https://doi.org/10.1016/j.bbcan.2020.188430.

50. Yin, J., Sheng, B., Qiu, Y., Yang, K., Xiao, W., and Yang, H. (2016). Role of AhR in positive regulation of cell proliferation and survival. Cell Prolif. *49*, 554–560. https://doi.org/10.1111/cpr.12282.

51. Franken, H., Mathieson, T., Childs, D., Sweetman, G.M.A., Werner, T., Tögel, I., Doce, C., Gade, S., Bantscheff, M., Drewes, G., et al. (2015). Thermal proteome profiling for unbiased identification of direct and indirect drug targets using multiplexed quantitative mass spectrometry. Nat. Protoc. *10*, 1567–1593. https://doi.org/10.1038/nprot.2015.101.

52. Ha, J., Park, H., Park, J., and Park, S.B. (2021). Recent advances in identifying protein targets in drug discovery. Cell Chem. Biol. *28*, 394–423. https://doi.org/10.1016/j.chembiol.2020.12.001.

53. Zampieri, M., Zimmermann, M., Claassen, M., and Sauer, U. (2017). Nontargeted Metabolomics Reveals the Multilevel Response to Antibiotic Perturbations. Cell Rep. *19*, 1214–1228. https://doi.org/10.1016/j.celrep.2017.04.002.

54. Pan, X., Qu, K., Yuan, H., Xiang, X., Anthon, C., Pashkova, L., Liang, X., Han, P., Corsi, G.I., Xu, F., et al. (2022). Massively targeted evaluation of therapeutic CRISPR off-targets in cells. Nat. Commun. *13*, 4049. https://doi.org/10.1038/s41467-022-31543-6.

55. Wienert, B., Wyman, S.K., Richardson, C.D., Yeh, C.D., Akcakaya, P., Porritt, M.J., Morlock, M., Vu, J.T., Kazane, K.R., Watry, H.L., et al. (2019). Unbiased detection of CRISPR off-targets in vivo using DISCOVER-Seq. Science *364*, 286–289. https://doi.org/10.1126/science.aav9023.

56. Lingeman, E., Jeans, C., and Corn, J.E. (2017). Production of Purified CasRNPs for Efficacious Genome Editing. Curr. Protoc. Mol. Biol. *120*, 31.10.1–31.10.19. https://doi.org/10.1002/cpmb.43.

57. Lin, S., Staahl, B.T., Alla, R.K., and Doudna, J.A. (2014). Enhanced homology-directed human genome engineering by controlled timing of CRISPR/Cas9 delivery. Elife *3*, e04766. https://doi.org/10.7554/eLife.04766.

58. Clement, K., Rees, H., Canver, M.C., Gehrke, J.M., Farouni, R., Hsu, J.Y., Cole, M.A., Liu, D.R., Joung, J.K., Bauer, D.E., and Pinello, L. (2019). CRISPResso2 provides accurate and rapid genome editing sequence analysis. Nat. Biotechnol. *37*, 224–226. https://doi.org/10.1038/s41587-019-0032-3.

59. Rhiel, M., Geiger, K., Andrieux, G., Rositzka, J., Boerries, M., Cathomen, T., and Cornu, T.I. (2023). T-CAST: An optimized CAST-Seq pipeline for TALEN confirms superior safety and efficacy of obligate-heterodimeric scaffolds. In Front Genome, *5*, 5, pp. 1130736. https://doi.org/10.3389/fgeed.2023.1130736.

Please cite this article in press as: Ursch et al., Modulation of TCR stimulation and pifithrin-α improves the genomic safety profile of CRISPR-engineered human T cells, Cell Reports Medicine (2024), https://doi.org/10.1016/j.xcrm.2024.101846

STAR★METHODS

KEY RESOURCES TABLE

REAGENT or RESOURCE	SOURCE	IDENTIFIER
Antibodies		
αCD3 (clone UCHT1)	BioLegend	Cat#: 300465; RRID:AB_2616677
αCD28 (clone CD28.2)	BioLegend	Cat#: 302943; RRID:AB_280074
αCD4-PB (clone SK3)	BioLegend	Cat#: 344620; RRID:AB_2228841
αCD8-APC (clone SK1)	BioLegend	Cat#: 344722; RRID:AB_2075388
αCD45RA-AF488 (clone HI100)	BioLegend	Cat#: 304114; RRID: AB_528816
αCCR7-PE (clone G043H7)	BioLegend	Cat#: 353204; RRID: AB_10913813
αPD-1-APC (clone EH12.2H7)	BioLegend	Cat#: 329908; RRID: AB_940475
αCXCR4-BV421 (clone 12G5)	BioLegend	Cat#: 306518;RRID: AB_11146018
αTCRα/β-PE (clone IP26)	BioLegend	Cat#: 306707; RRID: AB_314645
Dynabeads Human T-Activator CD3/CD28	Gibco	Cat#: 11132D
Immunocult Human CD3/CD28 T cell activator	Stemcell Technologies	Cat#: 10990
Biological samples		
buffy coats/human peripheral blood mononuclear cells (PBMCs)	German Heart Center Munich	N/A
Chemicals, peptides, and recombinant proteins		
cyclic pifithrin-α (hydrobromide)	MedChemExpress	Cat#: HY-15484
pifithrin-μ	Calbiochem	Cat#: 506155
Recombinant human IL-2	Peprotech	Cat#: 200-02
Recombinant human IL-7	Peprotech	Cat#: 200-07
Recombinant human IL-15	Peprotech	Cat#: 200-15
Recombinant *S.pyrogenes* Cas9-NLS protein	in-house[56,57]	N/A
CFSE	BioLegend	Cat#: 423801
DNA Quick Extraction solution	Biosearch Technologies	Cat#: 101094
RetroNectin	Takara	Cat#: T100B
Critical commercial assays		
MojoSort™ Human CD4 T cell Isolation Kit	BioLegend	Cat#: 480130
MojoSort™ Human CD8 T cell Isolation Kit	BioLegend	Cat#: 480129
P3 Primary Cell 96-well Nucleofector® Kit	Lonza Bioscience	Cat#: V4SP-3960
FOXP3 Fix/Perm Buffer Set	BioLegend	Cat#: 421403
DNeasy Blood & Tissue Kit	Qiagen	Cat#: 69504
NEBNext Ultra II FS DNA Library Prep Kit for Illumina	NEB	Cat#: E7805S
Single-Cell Core freeze buffer	Single-Cell Core	N/A
MiSeq Reagent Nano Kit v2 (500-cycles)	Illumina	Cat#: MS-103-1003
Deposited data		
Amplicon NGS data	GEO: GSE249934	N/A
CAST-Seq data	GEO: GSE249194	N/A
scKaryo-seq data	EGA: EGAS50000000656	N/A
Experimental models: Cell lines		
RD114	in-house	N/A
Nalm6 ffluc-GFP	Stanley Riddell; Fred Hutch Cancer Center	N/A

(*Continued on next page*)

Continued

REAGENT or RESOURCE	SOURCE	IDENTIFIER
Experimental models: Organisms/strains		
Mouse: NSGS (NOD.Cg-Prkdcscid Il2rgtm1Wjl Tg(CMV-IL3,CSF2,KITLG)1Eav/MloySzJ)	The Jackson Laboratory	JAX:013062
Oligonucleotides		
Alt-R CRISPR-Cas9 tracrRNA	IDT	Cat#. 1072534
Alt-R CRISPR-Cas9 crRNA	IDT	N/A
See Table S1	This paper	N/A
Recombinant DNA		
JCAR017 (clone FMC63) in pMP72	Juno Therapeutics GmbH, a Bristol-Myers Squibb Company	N/A
Cas9 expression plasmid pMJ915	Lin et al.[57]	Addgene; plasmid #69090
Software and algorithms		
D-CAST-Seq	Klermund et al.[41]	https://github.com/AG-Boerries/CAST-Seq
Aneufinder	Bakker et al.[43]	http://bioconductor.org/packages/AneuFinder/
CRISPResso (version 2.2.7)	Clement et al.[58]	http://crispresso2.pinellolab.org/submission
FlowJo (version 10.8.0)	FlowJo, LLC	https://www.flowjo.com
CytExpert 2.3	Beckman Coulter	https://www.beckman.de/flow-cytometry/research-flow-cytometers/cytoflex/software
GraphPad Prism 10 (version 10.3.1)	Graphpad	https://www.graphpad.com

EXPERIMENTAL MODEL AND STUDY PARTICIPANT ANALYSIS

Mouse model

NSGS mice (NOD.Cg-Prkdcscid Il2rgtm1Wjl Tg (CMV-IL3,CSF2,KITLG)1Eav/MloySzJ) (female, 6–8 weeks old, 18–22 g) were acquired from The Jackson Laboratory and kept at the mouse facility at the Technical University Munich, Institute for Medical Microbiology, Immunology and Hygiene. The mice were housed in groups under special, pathogen-free conditions at a constant temperature of 20°C with constant availability of food and water and subjected to a 12:12 days/night cycle. Littermates of the same sex were randomly allocated to the experimental groups. The performed animal experiments were approved by the district government of Upper Bavaria (Department 5—Environment, Health and Consumer Protection ROB-55.2-2532.Vet_02-18-162).

Primary human T cells

Buffy coats were collected by the German Heart Center Munich, with the approval of the local institutional review board (Ethics Committee TUM School of Medicine, Technical University of Munich) and with the informed consent of the patients. Information about age and gender of donors is not available. The study conforms to the standards of the Declaration of Helsinki. PBMCs were isolated using gradient density centrifugation with Pancoll (PAN-Biotech) and cultured in cRPMI as described in detail below.

METHOD DETAILS

Isolation and culture of primary human T cells

PBMCs were isolated out of buffy coats using gradient density centrifugation with Pancoll (PAN-Biotech) in SepMate 50 tubes at 1200 g for 20 min (Stemcell Technologies). The PBMC-containing supernatant was transferred into new falcons and washed with EasySep buffer (PBS (PAN-Biotech) with 2% FBS (Sigma-Aldrich)). PBMCs were enriched for CD4 or CD8 T cells using MojoSort Human CD4 T cell Isolation Kit (BioLegend) or MojoSort Human CD8 T cell Isolation Kit (BioLegend), respectively. The freshly obtained T cells were cultured in complete Roswell Park Memorial Institute (cRPMI) medium, consisting of RPMI 1640 (Gibco) supplemented with 5 mmol/L HEPES (PAN Biotech), 2 mmol/L glutamine (PAN Biotech), 50 μg/mL penicillin/streptomycin (PAN Biotech), 5 mmol/L nonessential amino acids (PAN Biotech), 5 mmol/L sodium pyruvate (PAN Biotech) and 10% FBS (Sigma-Aldrich) at a concentration of $1x10^6$ cells/ml for 24–48 h at 37°C before Cas9 RNP nucleofection. Freshly isolated CD4 T cells were optionally stained with αCD4-PB (clone SK3; BioLegend), αCD8-APC (clone SK1; BioLegend), αCD45RA-AF488 (clone HI100; BioLegend), αCCR7-PE (clone G043H7; BioLegend) and propidium iodide (BioLegend) for isolation of CCR7+CD45RA+ TN, CCR7-CD45RA- TEM and

CCR7+CD45RA- TCM cells by flow cytometry on a FACSAria III (software FACS Diva 8.0; Becton Dickinson) or a MoFlo Astrios EQ cell sorter (software Summit 6.3; Beckman Coulter). Optionally, frozen PBMCs (freezing medium: FBS +10% DMSO (Sigma-Aldrich)) were thawed, rested overnight in cRPMI and T cells were isolated the following day as described before.

Cas9 RNP assembly and nucleofection

100 μM Alt-R CRISPR-Cas9 crRNA (IDT) and 100 μM Alt-R CRISPR-Cas9 tracrRNA (IDT) were mixed in a 1:1 ratio and incubated for 5 min at 96°C to generate crRNA:tracrRNA duplexes (gRNA protospacer sequences: Table S1). An equal volume of 40 μM *Streptococcus pyrogenes* Cas9-NLS (made in-house[56,57]; Cas9 expression plasmid pMJ915 (Addgene)) was carefully added to the crRNA-tracrRNA duplex and incubated for 20 min at room temperature (RT) to generate Cas9 RNPs. $1x10^6$ cells were resuspended in 20 μL P3 buffer with Supplement 1 (LONZA) and 4 μL Cas9 RNP and 1 μL of 100 μM electroporation enhancer (Sigma-Aldrich) were added. T cells were nucleofected in 96-well reaction cuvettes (LONZA) using program EH-115 on the Lonza 4D-Nucleofector (LONZA). Directly after nucleofection, 80 μL cRPMI were added to the reaction cuvette. After resting for 30 min at 37°C the cells were transferred to a 96 well-plate and either activated with Dynabeads Human T-Activator CD3/CD28 (Gibco) in a cell:bead ratio of 10:1 and cultured with 100 U/ml IL-2 (Peprotech) or cultured with 0.5 ng/mL IL-7 (Peprotech) and 0.5 ng/mL IL-15 (Peprotech) (“non-activated” T cells). Alternatively, CD8 T cells were activated 48 h before nucleofection with Dynabead Human T-Activator CD3/CD28 in a cell:-bead ratio of 1:1 with or without the addition of 0.5 ng/mL IL-7 and 0.5 ng/mL IL-15 or with 5 μL Immunocult Human CD3/CD28 T cell Activator (Stemcell Technologies) per $1x10^6$ cells. IL-2 was replenished on day 6 of culture. 0.5 μM PFT-μ (Calbiochem) or 30 μM cyclic PFT-α (MedChemExpress) were added directly after nucleofection in the resting medium, as well as in the cultivation medium.

For sequential Cas9 RNP editing, $1x10^6$ cells/ml enriched CD4 T cells were activated on αCD3-coated 48 well-plate (10 μg/mL; clone UCHT1; BioLegend) in cRPMI with 5 μg/mL αCD28 (clone CD28.2, BioLegend) and 100 U/ml IL-2 for 48 h. For nucleofection, cells were resuspended in 100 μL P3 buffer with Supplement 1 and nucleofected with 20 μL Cas9 RNP and 5 μL electroporation enhancer in a 4D nucleocuvette (LONZA). Five days after initial CRISPR editing, cells were resuspended at a cell concentration of $1x10^6$ cells/ml and activated with 1 μL Immunocult Human CD3/CD28 T cell Activator per 1×10^6 T cells. Two days later a second CRISPR editing was performed with $1.8x10^6$ cells/nucleofection in 96-well reaction cuvettes as described before.

For *CD4*/*PDCD1*-double CRISPR editing for CAST-Seq analysis, Cas9 RNP nucleofection was performed in 4D nucleocuvette with 20 μL *CD4* Cas9 RNP in combination with 20 μL *PDCD1*-targeting Cas9 RNP and 5 μL electroporation enhancer.

CFSE T cell proliferation assay

T cells were washed twice with PBS and resuspended at $1x10^6$/mL in 1 μM CFSE (BioLegend) in PBS for 20 min in the dark at RT. The staining reaction was stopped by adding cRPMI and an additional incubation of 10 min. After two washing steps with PBS, the T cells were resuspended in P3 buffer with Supplement 1 and subjected to Cas9 RNP nucleofection as described before. After Cas9 RNP nucleofection T cells were stimulated with Dynabeads Human T-Activator CD3/CD28 in a cell:bead ratio of 10:1. T cells were sorted dependent on the CFSE dilution pattern and optional target protein expression at day 4–7 after nucleofection.

Flow cytometry analysis

Pre-enriched CD4 or CD8 T cells were stained with the following antibodies: αCD4-PO (clone: RPA-T4; Invitrogen), αCD4-PE, αCD4-PB or αCD4-BV785 (clone SK3; BioLegend), αCD3-BV785 or αCD3-PE (clone SK7; BioLegend), αPD-1-APC or αPD-1-BV650 or αPD-1-PE (clone EH12.2H7; BioLegend), αCD8-BV785, αCD8-APC/Fire or αCD8-PE/Dazzle594 (clone SK1; BioLegend), αCXCR4-BV421 or αCXCR4-PE (clone 12G5; BioLegend), αCD45RA-PE/Cy7, αCD45RA-AF488, or αCD45RA-BV421 (clone HI100; BioLegend), αCD45-PB (clone: T29/33; Dako), αCCR7-PE (clone G043H7; BioLegend), αTCRα/β-PE or αTCRα/β-APC (clone IP26, BioLegend), αCD19-PE/Dazzle 594 (clone: HIB19; BioLegend), αEGFR-PE (clone: AY13; BioLegend), FITC Streptavidin (BioLegend), αIFNγ-BV785, αIFNγ-PE/Cy7 (clone 4S.B3; BioLegend) or αIFNγ-PB (clone B27; BioLegend), αTNFα-PE/Cy7 or αTNFα-BV421 (clone MAb11; BioLegend), αIL-2-BV650 or αIL-2-BV510 (clone MQ1-17H12; BioLegend). To determine live cells Zombie NIR Fixable Viability Kit (BioLegend), Zombie Aqua Fixable Viability Kit (BioLegend) or propidium iodide (BioLegend) were applied according to the manufacturer’s recommendations. To determine the absolute KO cell numbers optionally 123count eBeads Counting Beads (Invitrogen) were added.

For cytokine staining cells were resuspended in cRPMI with 6.25 ng/mL phorbol 12-myristate 13-acetate (PMA; Sigma-Aldrich), 1 μg/mL ionomycin (Sigma-Aldrich) and 1:1200 GolgiPlug (BD Biosciences) and incubated for 5 h at 37°C. Cells were stained extracellularly for 30 min at 4°C in PBS. For additional intracellular staining the FOXP3 Fix/Perm Buffer Set (BioLegend) was used. T cells were resuspended in Fix&Perm buffer (BioLegend) and incubated for 30 min at RT. Cells were washed with Perm buffer (BioLegend) followed by the intracellular staining step in Perm buffer for 30 min at RT. Cells were washed twice with FACS buffer before analysis on a Cytoflex LX or S instrument (software CytExpert 2.3; Beckman Coulter).

Flow cytometry cell sorting and DNA extraction

T cells were stained with surface antibodies for 30 min and sorted based on the targeted gene and/or the CFSE dilution pattern on a FACSAria III (software FACS Diva 8.0; Becton Dickinson) or a MoFlo Astrios EQ cell sorter (software Summit 6.3; Beckman Coulter). Sorted cells were resuspended in DNA Quick Extraction solution (Biosearch Technologies) to lyse the cells and extract genomic DNA. The cell lysate was incubated at 65°C for 6 min, then 95°C for 2 min, and stored at −20°C.

Retrovirus production

1.2x10^6 RD114 cells were seeded in 3 mL DMEM (PAN Biotech) supplemented with 10% FCS and 50 μg/mL penicillin/streptomycin in one well of a 6-well plate 16–18 h before transfection. 18 μg plasmid (JCAR017 in pMP72; scFv sequence of JCAR017 (clone: FMC63) was kindly provided by Juno Therapeutics – a Bristol Myers Squibb company). DNA templates for retroviral transduction were designed in silico and synthesized by Twist Bioscience and 15 μL 3.31 M $CaCl_2$ solution were mixed with H_2O to a final volume of 150 μL. While vortexing the mixture was added dropwise to 150 μL of transfection buffer (1.6 g NaCl, 74 mg KCl, 50 mg H_2PO_4, 1 g HEPES in final 100 mL H_2O, pH 6.76). After 20 min at RT the transfection mixture was added dropwise to RD114 cells. Medium was exchanged after 6 h with cRPMI medium. Virus was harvested after 48 and 72 h.

CAR T cell engineering

T cells were stimulated with 5 μL Immunocult Human CD3/CD28 T cell Activator per 1x10^6 cells in cRPMI supplemented with 100 U/ml IL-2. After 48 h, CD8 and CD4 CAR T cells were nucleofected separately with Cas9 RNPs using the nucleofection code DK-100. After nucleofection, cells were treated with either DMSO or PFT-α as described before and restimulated with 5 μL Immunocult Human CD3/CD28 T cell Activator per 1x10^6 cells and 100 U/ml IL-2. After 48 h cells were transduced with the retroviral anti-CD19-CAR construct. Non-treated 24-well tissue culture plates were coated with 0.06 μg/mL RetroNectin (Takara) in 300 μL PBS per well. 900 μL retrovirus were centrifuged on the RetroNectin-coated wells for 2 h at 3000 g and 32°C. 700 μL of the supernatant was replaced with 700 μL T cell suspension in cRPMI with 100 U/ml IL-2 (0.5x10^6 cells/well). After one week of expansion, CAR-positive cells were enriched using the MojoSort Human anti-APC Nanobeads kit (BioLegend) in combination with αEGFR-APC antibody (clone AY13, BioLegend).

In vitro killing assay

Enriched CD8 CAR T cells were activated with 5 μL Immunocult Human CD3/CD28 T cell Activator per 1x10^6 cells and 100 U/ml IL-2 and cultured for two days in cRPMI. 2x10^4 CAR CD8 T cells were cocultured with Nalm6 ffluc-GFP tumor cells in T cell: tumor cell ratios of 1:1, 1:2 and 1:4 or without tumor cells as a negative control. All cultures were performed in technical duplicates. After 4 and 24 h the flow cytometry readout was performed. Results of DMSO and PFT-α conditions were normalized for differences in transduction rates.

Nalm6 *in vivo* tumor model

0.5x10^6 Nalm6 ffluc-GFP (firefly luciferase) tumor cells were transferred to 6–8 week old NSGS mice 7 days before CAR T cell transfer. Two days prior CAR T cell injection, CAR T cells were restimulated with 5 μL Immunocult Human CD3/CD28 T cell Activator per 1x10^6 cells and 100 U/ml IL-2. A total of 8x10^6 CAR T cells (CD8:CD4 ratio 1:4) in 100 μL PBS per mouse were used. Mock mice received the equal amount of non-edited, untransduced T cells. For tumor progression, bioluminescence imaging of tumor cells was conducted. Therefore, mice were intraperitoneally injected with 150 mg/kg XenoLight D-Luciferin Potassium Salt dissolved in PBS (PerkinElmer). After 5 min, mice were anesthetized with 2.5% isoflurane RAS-4 Rodent Anesthesia system (PerkinElmer) and imaged in the IVIS Lumina Imaging System (PerkinElmer LAS). The analysis was performed by quantification of photons/sec/cm^2/sr with Living Image 4.5 software (PerkinElmer). Imaging was conducted on days 6 and 9, simultaneously to blood sampling. Additionally, bone marrow and spleen were analyzed on day 9. For erythrocyte lysis, 100 μL blood were incubated with 10 mL ACT buffer (0.15 M Ammonium chloride, 17 mM TRIS) for 10 min, washed and reincubated with 5 mL ACT buffer for another 5 min. Bone marrow was obtained from femurs and incubated with 3 mL ACT for 3 min. Spleens were mashed through a 100 μm cell sieve and treated with 5 mL ACT buffer for 5 min. FACS staining was performed as mentioned before.

CAST-seq analysis

Genomic DNA (gDNA) was extracted using the DNeasy Blood & Tissue Kit (Qiagen) according to the manufacturer's protocol. CAST-Seq analyses were performed as previously described,[44] with few modifications: In brief, 250 ng of genomic DNA were used as input material for each analysis. Libraries were prepared using the NEBNext Ultra II FS DNA Library Prep Kit for Illumina (NEB). Enzymatic fragmentation of the genomic DNA was aimed at an average length of 500–800 bp.[44] CAST-Seq libraries were sequenced on a NovaSeq 6000 using 2x 150 bp paired-end sequencing (GENEWIZ, Azenta Life Sciences). For each treatment, CAST-Seq was performed with gDNA from three independent donors. Only sites that were detected as significant hits in two replicates were further analyzed by targeted amplicon sequencing. CAST-seq primers are listed in Table S1 (translocation events and large deletions at the CD4 locus were sequenced). CAST-Seq results are provided in Table S3. The D-CAST-Seq bioinformatic pipeline for the simultaneous use of two gRNAs was used.[41] For sites under investigation the spacer sequence of the gRNA was aligned to the most covered regions for each site (±200 bp).[59] Sites were labeled as OMT if any of the two *p*-values reached the cut-off of 0.005.[41]

CAST-Seq read coverage was plotted as follows: the +/− 5 kb window around the on-target site was divided into bins of 100 bp, and all reads falling in a respective bin were displayed as log2 read counts per million (CPM). Quantifications of the CAST-Seq coverage plots were calculated the following way: % large aberrations = sum of all reads in bins >200 bp from the cleavage site/sum of all reads in all bins. Mean deletion length = sum of (count of deletion reads * distance from the cleavage site)/sum of all deletion reads. Deletion reads are all 'negative' reads in CAST-Seq read orientation (Table S3).

Please cite this article in press as: Ursch et al., Modulation of TCR stimulation and pifithrin-α improves the genomic safety profile of CRISPR-engineered human T cells, Cell Reports Medicine (2024), https://doi.org/10.1016/j.xcrm.2024.101846

ddPCR

For ddPCR, 67.5 ng of genomic DNA were added to the ddPCR reaction mix containing QX200TM EvaGreen ddPCR Supermix (Bio-Rad). Each reaction was performed with 100 nM of primers (primer sequences are listed in Table S1) and loaded into the QX200 Droplet Generator (Bio-Rad). The generated droplets were transferred to a 96-well PCR plate (Bio-Rad) and the plate sealed with a PX1 PCR plate sealer (Bio-Rad). Endpoint PCR was performed with the following program: 95°C for 5 min, 40 cycles of 95°C for 30 s, 66°C for 1 min, 72°C for 1 min, followed by 5 min at 4°C and 5 min at 90°C (ramping rate set to 2 °C/s). Data was acquired in a QX200 Droplet Reader and results analyzed with QuantaSoft Analysis Pro (Bio-Rad).

CD4-PDCD1 translocation events leading to chromosomes with one centromere (reciprocal translocations) or two centromeres (non-reciprocal translocations) were detected with two different primer sets, and two technical replicates were run for each primer set and each sample. To calculate the frequencies of translocations, the translocation ddPCR values were first corrected for noise (subtraction of value of untreated matched control) and then normalized for the amount of genomic input DNA (positive droplets of control amplicon on chr11). The overall translocation frequency is displayed as the sum of the events for reciprocal and non-reciprocal translocations.

scKaryo-seq analysis

CD8 T cells were activated for 48 h with antiCD3/CD28-coated beads in a cell:bead ratio of 1:1 and nucleofected with *TRAC*-targeting Cas9 RNPs as described before. After 5 days in culture, KO T cells were stained with αhTCRα/β-PE (clone IP26; BioLegend), αCD8-FITC (clone RPA-T8; BioLegend) and Zombie Aqua (BioLegend) for 30 min and single cell flow-sorted into 384 well-plates with 5 μL of mineral oil/well (Sigma-Aldrich) with a FACSAria III cell sorter (software FACS Diva 8.0; Becton Dickinson). Immediately after sorting plates were stored at −80°C. Non-activated *TRAC* KO CD8 T cells were generated as described before. At day 5 after nucleofection live KO cells were flow-sorted into 1.5 mL Protein LoBind tubes. Cells were washed twice with PBS and pellet was resuspended in 125μL PBS. 375μL 100% Ethanol (pre-cooled to −20°C) was added and the tube was stored for 1 h at −20°C. Cells were pelleted, resuspended in 0.5 mL of Single-Cell Core freeze buffer and stored at −80°C. Final cell sorting into 384 well-plates was performed by Single-Cell Core of the Oncode Institute, Utrecht, the Netherlands. scKaryo-seq libraries were prepared at the SingleCell core facility of the Oncode Institute, Utrecht, the Netherlands, and sequenced on a NextSeq2000 2x100 bp paired-end sequencing (Illumina). scKaryo-seq data were processed for copy number analysis using Aneufinder.[43] Segments on binned counts (2 MB) were identified using the Aneufinder algorithm with the method 'edisive' and 100 random permutations. The algorithm is executed on all autosomes and GC correction is enabled. Single cells are then clustered using the Aneufinder ''clusterByQuality'' function and split into a set of higher and lower quality cells.[43] Only high-quality cells are presented in Figures 6F, S6C, and S6D. In Figures S6A and S6B the overall sequencing quality was higher and no split into higher/lower quality cells was performed. In Table S4, ''Gains''/''Losses'' and breakpoints are recorded.

Amplicon NGS

The indel patterns of CRISPR/Cas9-edited human T cells were determined by amplicon sequencing followed by NGS. Primers were designed to result in an amplicon length of 350–500 bp using Benchling (Table S1). A 25 μL PCR reaction contained 10 μL of genomic DNA, 0.5 μL 10 μM primer forward, 0.5 μL 10 μM primer reverse, 12.5 μL 2x GoTaq Long PCR Master Mix (Promega) and 1.5 μL H_2O. The thermocycler setting consisted of one step at 95°C for 1 min; followed by 18 cycles at 98°C for 10 s, 65°C for 15 s and 72°C for 15 s (wherein the annealing temperature was decreased by 0.5°C per cycle); followed by 15 cycles at 98°C for 10 s, 58°C for 15 s and 72°C for 15 s; with one final step at 72°C for 5 min. The PCR products were cleaned up using AMPure beads according to the manufacturer's recommendations (Beckmann Coulter) and eluted in 50 μL 10 mM Tris. For barcoding, 2 μL of the purified DNA were added to 10 μL of 2x GoTaq Long PCR Master Mix, 2 μL of Nextera XT index 1 (i7) primer, 2 μL of Nextera XT index 2 (i5) primer (Illumina) and 4 μL of H_2O. The PCR reactions were heated up to 95°C for 3 min, followed by 8 cycles of 95°C for 30 s, 55°C for 30 s and 72°C for 30 s and a further elongation step for 5 min at 72°C. The second PCR products were again purified with AMPure beads and eluted in 27.5 μL 10 mM Tris. Cleaned-up PCR products were quantified using the SpectraMax Quant AccuBlue HighRange dsDNA Kit (Molecular Devices) on the SpectraMax 3x instrument (Molecular Devices). Equal amounts of DNA/sample were pooled and sequenced on an Illumina MiSeq instrument (Illumina) with a MiSeq Reagent Nano Kit v2 (500-cycles) (Illumina) according to the manufacturer's recommendations. NGS sequencing results were analyzed using CRISPResso (version 2.2.7) with the following prompt: CRISPRessoBatch –batch_settings [name.batch] –amplicon_seq [sequence amplicon] -g [sequence gRNA] -n nhej -gn [name gRNA] -w 0 –skip_failed -o [name of output folder].[58] To determine KO efficiencies the setting -w 30 was used. The resulting distribution of deletions or insertions was visualized using GraphPad Prism 10. For descriptive statistics, the data were transformed using RStudio (version 2023.03.1 + 446, Posit Software) to enable the calculation of the mean and the 95%-confidence interval (95-CI) of the deletion size as well as the use of the Wilcoxon signed-rank test or Friedman test to check for differences between the different populations (Table S2).

QUANTIFICATION AND STATISTICAL ANALYSIS

Flow cytometry data were analyzed using FlowJo v10.8.0. Statistical tests were selected based on the dataset and performed in GraphPad Prism 10 Statistical test and biological replicates are indicated in figure legends. A p-value of <0.05 was considered statistically significant.